NOLTR 73-162

NOL TECHNICAL REPORT

ANALYSIS OF RIGID POLYURETHANE FOAM AS A SHOCK MITIGATOR

BY
William M. Hinckley
J.C.S. Yang

NAVAL ORDNANCE LABORATORY
WHITE OAK, SILVER SPRING, MD. 20910

6 AUGUST 1973

- Approved for public release;distribution unlimited

NAVAL ORDNANCE LABORATORY
WHITE OAK, SILVER SPRING, MARYLAND 20910

UNCLASSIFIED
Security Classification

DOCUMENT CONTROL DATA - R & D

Security classification of title, body of abstract and indexing annotation must be entered when the overall report is classified)

1 ORIGINATING ACTIVITY (Corporate author)	2a. REPORT SECURITY CLASSIFICATION
Naval Ordnance Laboratory Silver Spring, Maryland 20910	UNCLASSIFIED 2b. GROUP

3 REPORT TITLE

Analysis of Rigid Polyurethane Foam as a Shock Mitigator

4. DESCRIPTIVE NOTES (Type of report and inclusive dates)

5. AUTHOR(S) (First name, middle initial, last name)

William M. Hinckley and J. C. S. Yang

6. REPORT DATE	7a. TOTAL NO. OF PAGES	7b. NO. OF REFS
6 August 1973	75	10

8a. CONTRACT OR GRANT NO	9a. ORIGINATOR'S REPORT NUMBER(S)
ORD-35A-001/UR02-303-003 b. PROJECT NO.	NOLTR 73-162
c.	9b. OTHER REPORT NO(S) (Any other numbers that may be assigned this report)
d.	

10. DISTRIBUTION STATEMENT

Approved for public release; distribution unlimited.

11. SUPPLEMENTARY NOTES	12. SPONSORING MILITARY ACTIVITY
	Naval Ordnance Systems Command Washington, D. C. 20360

13. ABSTRACT

In problems of water impact, the compressive stress wave generated in a weapon vehicle at the surface of contact can be quite severe. In certain instances it may be necessary to mitigate the peak stress. Many materials, e.g., rigid polyurethane foam, exhibit elastic, nearly perfectly plastic stress-strain relations. Stresses greater than the yield stress cannot be transmitted until compaction occurs.

The purpose of this report is to investigate the mitigation of shock and absorption of energy under impact-loading conditions through the use of crushable materials. Experimental data are presented on the mitigated impacts of a short steel projectile on a long aluminum rod. A theoretical analysis is formulated and the results are compared with the experimental results. Mitigators of varying cross-sectional area, as well as mitigators of constant cross-sectional area, are included. The dynamic properties of the rigid polyurethane foam were obtained experimentally and from the literature and used as input for the theoretical analysis.

14. KEY WORDS	LINK A		LINK B		LINK C	
	ROLE	WT	ROLE	WT	ROLE	WT
polyurethane						
foam						
shock mitigation						
stress						
strain						
strain rate						
dynamic						
testing						
energy absorption						
water entry						

ANALYSIS OF RIGID POLYURETHANE FOAM AS A SHOCK MITIGATOR

Prepared by:
William M. Hinckley and J. C. S. Yang

ABSTRACT: In problems of water impact, the compressive stress wave generated in a weapon vehicle at the surface of contact can be quite severe. In certain instances it may be necessary to mitigate the peak stress. Many materials, e.g., rigid polyurethane foam, exhibit elastic, nearly perfectly plastic stress-strain relations. Stresses greater than the yield stress cannot be transmitted until compaction occurs.

The purpose of this report is to investigate the mitigation of shock and absorption of energy under impact-loading conditions through the use of crushable materials. Experimental data are presented on the mitigated impacts of a short steel projectile on a long aluminum rod. A theoretical analysis is formulated and the results are compared with the experimental results. Mitigators of varying cross-sectional area, as well as mitigators of constant cross-sectional area, are included. The dynamic properties of the rigid polyurethane foam were obtained experimentally and from the literature and used as input for the theoretical analysis.

NAVAL ORDNANCE LABORATORY
SILVER SPRING, MARYLAND

NOLTR 73-162 6 August 1973

ANALYSIS OF RIGID POLYURETHANE FOAM AS A SHOCK MITIGATOR

This work was performed to investigate the mitigation of shock and absorption of energy under impact-loading conditions through the use of crushable materials with application to water-entry vehicles. The work was sponsored by the Naval Ordnance Systems Command under ORD-35A-001/UR02-303-003.

The authors wish to express their appreciation to the many individuals who assisted in this undertaking, especially Mr. J. M. Marshall for his assistance with the experiments and Dr. J. E. Goeller for his guidance.

ROBERT WILLIAMSON II
Captain, USN
Commander

A. E. Seigel

A. E. SEIGEL
By direction

CONTENTS

ILLUSTRATIONS

ILLUSTRATIONS (Cont'd)

TABLES

LIST OF SYMBOLS

a	-	acceleration; Lagrangian coordinate
A	-	cross-sectional or stress area
A_b	-	cross-sectional area of bar
A_s	-	cross-sectional area of specimen
C	-	constant for curve fitting
C_1	-	constant for curve fitting
C_2	-	constant for curve fitting
C_3	-	constant for curve fitting
D	-	diameter
D_1	-	initial diameter of tip of mitigator
D_2	-	initial diameter of base of mitigator
E	-	Young's modulus
E_A	-	energy absorbed by mitigator
F	-	force
g	-	elastic wave velocity
k	-	constant for curve fitting

k_1 - constant for curve fitting

k_2 - constant for curve fitting

L - length of mitigator or specimen

M - mass of projectile

t - time

T - pulse length

U - particle velocity

U_o - projectile impact velocity

U_r - projectile rebound velocity

U_1 - velocity of projectile-mitigator interface

U_{1_o} - initial velocity of projectile-mitigator interface

U_2 - velocity of mitigator-rod interface

U_{2_o} - initial velocity of mitigator-rod interface

V - volume

X - axial coordinate

X_1 - coordinate of projectile-mitigator interface

X_{1_o} - initial coordinate of projectile-mitigator interface

X_2 - coordinate of mitigator-rod interface

X_{2_o} - initial coordinate of mitigator-rod interface

ΔKE - change in kinetic energy

ΔSE - change in strain energy

ε - strain

ε_{avg} - average strain

ε_c - compaction strain

ε_r - reflected strain

ε_s - specimen strain

ε_t - transmitted strain

$\dot{\varepsilon}$ - strain rate

$\dot{\varepsilon}_s$ - specimen strain rate

ρ - initial density

σ - stress

σ_o - limit yield stress

σ_p - plateau stress

σ_s - average specimen stress

σ_y - yield stress

CHAPTER I

INTRODUCTION

In problems of water impact, the compressive stress wave generated in a weapon vehicle at the surface of contact can be quite severe. In certain instances it may be necessary to mitigate the peak stress so that some maximum allowable stress is not exceeded. This can be accomplished by protecting the contact surface with a crushable material. Consider, for example, the vertical water impact of a torpedo model on a calm water surface. When the nose enters the water unprotected, a short-duration high-amplitude stress pulse is generated which is nearly a linear function of the impact velocity, Figure 1. However, when protected by a crushable mitigator, the duration of the stress pulse is increased and the amplitude is decreased. The extent of mitigation can be substantial, as shown in Figure 1, but is dependent upon the mechanical properties of the crushable material chosen. For a particular weapon design and impact condition, the material properties of the mitigator should be optimized on the basis of allowable load, weight, volume, etc.

Many materials, e.g., rigid polyurethane foam, exhibit elastic, nearly perfectly plastic stress-strain relations until compaction occurs at large strains. Compaction refers to the closure of the pores in the foam to the extent that it behaves as a solid material. Stresses greater than the yield stress cannot be transmitted by such materials until compaction occurs. A typical compressive stress-strain curve for rigid polyurethane foam is presented in Figure 2. It is characterized by a low elastic modulus resulting in a gross yield strain on the order of 5 percent, near perfectly plastic behavior to large strain on the order of 50 percent, and subsequent increasing rigidity due to compaction. The unloading curve is characterized by an initially rapid decrease in stress with strain followed by a large recovery in strain at very low stress.

The purpose of this report is to investigate the mitigation of shock and absorption of energy under impact-loading conditions through the use of crushable materials. Experimental data are presented on the mitigated impacts of a short steel projectile on a long aluminum rod. A theoretical analysis is formulated and the results are compared with the experimental results. Since the geometry of systems subjected to impact loading is often dictated by other considerations, mitigators of varying cross-sectional area, such as conical frustums, as well as mitigators of constant cross-sectional area, are included.

The dynamic properties of the rigid polyurethane foam were obtained experimentally and used as input for the theoretical analysis. Functional formulations for the density and strain rate dependence of the elastic modulus, yield strength and plateau stress are established using these data obtained from experiments and from the literature. These empirical functions are used in a computer program to facilitate the prediction of mitigator performance under impact loading.

This report is divided into six sections:

1. In Chapter II, the theoretical stress-strain relations for the foam are formulated.

2. In Chapter III, the dynamic material property data are presented and the theoretical models are numerically fitted to these data.

3. In Chapter IV, the analytical treatment of the impact problem is discussed.

4. In Chapter V, the apparatus used for the dynamic stress-strain and the impact experiments are described.

5. In Chapter VI, the theoretical results are compared with the experimental data.

6. In Chapter VII, the conclusions are presented.

CHAPTER II

MATERIAL MODELS

Three theoretical stress-strain models are considered, Figure 3. The first is simply a rigid, perfectly plastic, locking model. The second is an elastic, perfectly plastic, compacting model. The third, an elastic, perfectly plastic, strain-rate dependent, compacting model, is a rate dependent version of the second.

RIGID, PERFECTLY PLASTIC, LOCKING MODEL

The rigid, perfectly plastic, locking model, hereafter referred to as the RPL model, is illustrated in Figure 3A. It ignores all elastic response of the material during loading and unloading. Any compressive strain up to the compaction strain produces a stress equal to the yield stress until unloading occurs. Unloading takes place with essentially no recovery in strain. Perrone, Reference 1, has used this model, with the addition of strain rate effects, to obtain a closed form solution for the dynamic response of a mass coupled to a rigid wall by a wire. Green, et al., Reference 2, found the yield stress for rigid polyurethane foam to be strain rate and density dependent. In Reference 3, Perrone points out that most of

the plastic work is done before the stress-strain rate point departs appreciably from its initial value. Therefore, the yield stress associated with the initial strain rate can be used for the entire calculation with little loss in accuracy and much simplification.

While this model may be acceptable for predicting plastic strain and energy absorption using the proper initial yield stress, it does not adequately describe the force-time and velocity-time curves generated during impact.

ELASTIC, PERFECTLY PLASTIC, COMPACTING MODEL

The elastic, perfectly plastic, compacting model, the EPC model, includes the addition of pre-yield elastic response, elastic unloading and post-compaction elastic response, Figure 3B. Schmidt and Hoffman, Reference 4, and Mustin, Reference 5, have presented the rigidity modulus for polyurethane foams as a function of temperature, Figure 4. These data indicate that since the rigid foams are in the glassy state at room temperature, the rigidity modulus is nearly temperature independent at that temperature. Schwaber and Meinecke, Reference 6, suggested that since these foams are in the glassy state, the modulus is also approximately strain rate independent. However, the modulus is highly density dependent and has been extensively studied under "quasi-static" loading by many of the manufacturers. Schwaber and Meinecke, Reference 6, also stated that the unloading stress-strain curve appears to be independent of strain rate. The slope of the unloading path is assumed to be equal to the slope of the initial elastic loading path because reliable experimental data on the actual unloading path are lacking. The large recovery in strain at very low stress, Figure 1, is ignored also because of insufficient data. However, this is not a serious deficiency except for multiple impacts. No multiple impacts are considered in this work. The post-compaction response is treated elastically here for convenience. In reality, the compaction process does not occur abruptly and the compaction strain is therefore a nebulous quantity, Figure 2. The transition is smooth and amenable to modeling, but data are not available on the density and strain rate dependence of the process. In general, the loading and unloading paths following the onset of compaction are not coincident.

ELASTIC, PERFECTLY PLASTIC, STRAIN RATE DEPENDENT, COMPACTING MODEL

The elastic, perfectly plastic, strain rate dependent, compacting model, the EPRC model, introduces a strain rate dependent plateau stress in addition to a strain rate dependent yield stress, Figure 3C. The elastic response remains strain rate independent, while the yield stress and yield strain become strain rate dependent, increasing with increasing rate. The plateau stress becomes a function of the instantaneous strain and strain rate. It will therefore differ from the yield stress for situations of varying

strain rate. The unloading path is again chosen as elastic with a slope equal to that of the initial elastic loading. However, for cases of equal maximum strain, the path is not unique except for cases of equal strain rate. Again, for convenience, the compaction strain is chosen as a discrete strain regardless of strain rate. The post-compaction loading and unloading path is also not unique except for cases of equal strain rate.

CHAPTER III

NUMERICAL FIT OF MODELS TO DATA

For the analysis, the following assumptions are made concerning the polyurethane foam material.

1. The elastic modulus is density dependent, but strain rate independent.

2. The yield stress and plateau stress are density dependent and strain rate dependent.

3. The unloading stress-strain relation is density dependent, but strain rate independent.

Material property data for rigid polyurethane foam have been obtained from stress-strain strain-rate tests and from the literature. Since foam materials are typically anisotropic at low densities, all data and test results apply to material loaded parallel to the direction of rise. The direction of rise is defined as the direction in which the foam is allowed to expand during fabrication.

As previously stated, the elastic modulus is assumed to be density dependent, but strain rate independent. Therefore, data acquired under "quasi-static" conditions are considered applicable to strain rates up to at least 1000 in./in./sec. Modulus data obtained according to ASTM D1621 are presented in Reference 7 as a function of density. These data are listed in Table 1. To facilitate the numerical computations, a curve of the form

$$E = C\rho^{k} \tag{1}$$

was fitted to these data. The resulting curve fit, Figure 5, is

$$E = 230\rho^{1.7} \tag{2}$$

where E is the elastic modulus in psi and ρ is the initial foam density in lbs./ft.^{3}.

The dynamic yield stress and the plateau stress at 20 percent strain, Figure 2, were determined experimentally as functions of

TABLE 1

COMPRESSIVE MODULUS OF RIGID POLYURETHANE FOAM

Tested According to ASTM D1621 at 74°F
in Direction Parallel to Rise

Density ($lbs./ft.^3$)	Compressive Modulus (psi)
3	1,020
4	2,100
6	4,400
8	7,700
10	11,500
12	16,000
14	21,000
16	26,000
20	38,000

From Reference 7

density and strain rate. Three densities of the foam - nominal 3.5, 7.0, and 14.5 lbs./ft.^{3} - were tested in compression at rates of strain between 10^{-2} and 10^4 in./in./sec. All of the test specimens were loaded parallel to the direction of rise. Each test was conducted at nearly constant strain rate. Varying densities, nonuniform cellular structures and flaws produced scatter in the data. Typical stress-strain curves are presented for various strain rates in Figures 6, 7, and 8 for each of the three densities. Note the drop in stress which occurs after yield. Since the material models omit the peak, a plateau stress - for example, the stress at 20 percent strain - is a better parameter to use in the analysis than the peak stress. To aid in determining the resultant trends, equations of the form

$$\sigma = (C_1 + C_2 \ln \dot{\varepsilon}) \rho^{k_1} \tag{3}$$

were fitted to the yield stress and plateau stress data by the method of least squares. $\dot{\varepsilon}$ is the average strain rate in the specimen in in./in./sec., ρ is the initial density of the specimen in lbs./ft.^{3} and C_1, C_2, and k_1 are the parameters adjusted to satisfy the least square condition. The equation developed to fit the yield stress data is

$$\sigma_y = (10.9 + .385 \ln \dot{\varepsilon}) \rho^{1.64} \tag{4}$$

and the equation developed to fit the plateau stress data is

$$\sigma_p = (8.69 + .306 \ln \dot{\varepsilon}) \rho^{1.69} \tag{5}$$

The density and strain rate dependence of these data and the fitted curves are illustrated in Figures 9, 10, 11, and 12.

CHAPTER IV

ANALYTICAL APPROACH

In formulating the analytical approach to this impact problem, the following assumptions are made:

1. The projectile is sufficiently rigid, compared to the mitigator, that it can be treated as a lumped mass which undergoes negligible deformation.

2. The mass of the mitigator and, hence, the inertia is negligible compared to that of the projectile.

Assumption (2) implies that the theoretical results will be the same for the case of a mitigator attached to the projectile and the case of a mitigator attached to the rod.

CONSTANT AREA MITIGATOR

The experimental configuration can be divided into three free body diagrams.

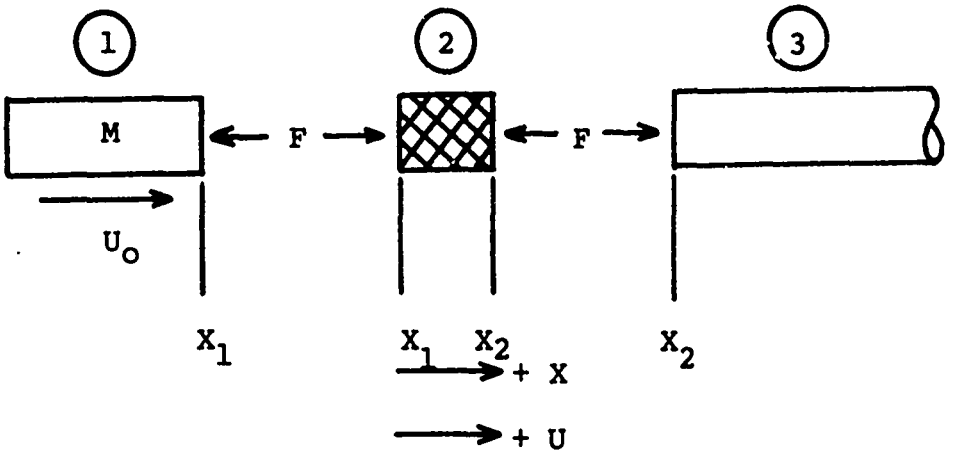

where

$$X_{1_o} = 0$$

$$X_{2_o} = L$$

$$U_{1_o} = U_o$$

$$U_{2_o} = 0$$

Summing the forces applied to the projectile in the axial or x-direction gives

$$-F = Ma \tag{6}$$

or

$$a = \frac{-F}{M} \tag{7}$$

where, in general,

$$F = F(\varepsilon, \dot{\varepsilon}, A)$$

ε = strain of the mitigator (8)

$\dot{\varepsilon}$ = strain rate of the mitigator

A = stress area of the mitigator

Integrating with respect to time gives the velocity relation

$$U_1 = U_o - \int_o^t \frac{F}{M}\, dt \tag{9}$$

Integrating again gives the distance traveled

$$X_1 = U_o T - \int_o^T \int^t \frac{F}{M}\, dtdt \tag{10}$$

by the projectile.

Utilizing the one-dimensional theory of finite amplitude wave propagation, the transient response of the rod to a force F applied to the end is given by

$$U_2 = \frac{F}{(\rho g A)_{rod}} \tag{11}$$

where

ρ = density of the rod material

g = elastic wave velocity in the rod

A = cross-sectional area of the rod

Integrating yields

$$X_2 = L + \int_o^T \frac{F}{(\rho g A)_{rod}} dt \tag{12}$$

The solution to this impact problem lies in determining $F(\varepsilon,\dot{\varepsilon},A)$ at each instant in time. To obtain this result, the strain and strain rate of the mitigator must also be determined at each instant in time. The engineering strain of the mitigator is given by

$$\varepsilon = \frac{L - (X_2 - X_1)}{L} \tag{13}$$

Substituting for X_1 and X_2 yields

$$\varepsilon = \frac{1}{L}\left[U_o T - \int_o^T \int_o^t \frac{F}{M}\, dt dt - \int_o^T \frac{F}{(\rho g A)_{rod}} dt\right] \tag{14}$$

The strain rate of the mitigator is given by

$$\dot{\varepsilon} = \frac{-(U_2 - U_1)}{L} \tag{15}$$

Substituting for U_1 and U_2 yields

$$\varepsilon = \frac{1}{L}\left[U_o - \int_o^T \frac{F}{M}\, dt - \frac{F}{(\rho g A)_{rod}}\right] \tag{16}$$

Using Equation (8) as a constraint, Equations (14) and (16) can then be integrated, see Appendix A, to determine the force-time curve, the strain-time curve of the mitigator, and the velocity-time curves of the projectile and the rod.

Of equal interest to the magnitude of the force transmitted by the mitigator is the amount of energy absorbed by the mitigator. For example, a soft elastic material will not dissipate as much energy as a soft plastic material. The strain energy absorbed by the mitigator, plus the kinetic energy and the strain energy imparted to the rod, equals the change in kinetic energy of the projectile during the impact. The final strain energy absorbed by the mitigator is then

$$E_A = \Delta KE_{proj} - \Delta KE_{rod} - \Delta SE_{rod} \tag{17}$$

where

$$\Delta KE_{proj} = \frac{1}{2} M(U_o^2 - U_r^2) \tag{18}$$

and from Reference 8

$$\Delta KE_{rod} = \frac{1}{2} (\rho g A)_{rod} \int_o^T U^2 dt \tag{19}$$

For a semi-infinite rod stressed below the elastic limit

$$U^2 = \frac{\sigma^2}{\rho^2 g^2} = \frac{E^2\epsilon^2}{\rho^2 g^2} = \frac{E\epsilon^2}{\rho} \qquad (20)$$

The change in kinetic energy becomes

$$\Delta KE_{rod} = \frac{1}{2} (AEg)_{rod} \int_o^T \epsilon^2_{rod}\, dt \qquad (21)$$

The strain energy imparted to the rod is

$$\Delta SE_{rod} = \frac{1}{2} \int_o^V \sigma\epsilon dV \qquad (22)$$

Substituting E ϵ for σ and Agdt for dV gives

$$\Delta SE_{rod} = \frac{1}{2} (AEg)_{rod} \int_o^T \epsilon^2_{rod} dt \qquad (23)$$

Equation 17 then becomes

$$E_A = \frac{1}{2} M(U_o^2 - U_r^2) - (AEg)_{rod} \int_o^T \epsilon^2_{rod}\, dt \qquad (24)$$

or

$$E_A = \frac{1}{2} M(U_o^2 - U_r^2) - \left(\frac{g}{AE}\right)_{rod} \int_o^T F^2\, dt \qquad (25)$$

VARYING AREA MITIGATOR

For many applications the mitigators are not of constant area, but rather are elements of varying area. Consider the conical frustum in Figure 13 to which an increasing load F(t) is applied. It is divided into N cylindrical discs of increasing cross-sectional area. Now consider just the disc N = 1. It undergoes elastic deformation until it reaches its yield strength, then perfectly plastic deformation until compaction occurs. At the same time, discs N = 2 through N = N undergo only elastic deformation because

of their larger stress areas. Following compaction, disc N = 1 can transmit a higher load. Disc N = 2 then yields, deforms plastically and compacts. This process continues until either the load is restricted or all of the elements have, in turn, yielded and compacted.

For stresses below the yield stress of disc N = 1, the load-carrying capability of the mitigator is

$$F = \sigma_1 A_1 \tag{26}$$

where $\sigma_1 \leq \sigma_y$ and A_1 is the cross-sectional area of disc N = 1. For stresses above the yield stress of disc N = 1, but below that of disc N = N

$$F = \sigma_y A_i \tag{27}$$

where A_i is the cross-sectional area of the disc, which is just loaded to its yield stress with limits

$$A_1 \leq A_i \leq A_N$$

The area A_i is given by

$$A_i = \frac{\pi}{4} D_i^2 \tag{28}$$

where D_i is the diameter of the mitigator at

$$X_i = \frac{\varepsilon_{avg}}{\varepsilon_c} L \tag{29}$$

and ε_{avg} and ε_c are defined as the average mitigator strain and the compaction strain of the material, respectively. For conical mitigators

$$D_i = D_1 + (D_2 - D_1) \left(\frac{X_i}{L}\right) \tag{30}$$

or

$$D_i = D_1 + (D_2 - D_1) \left(\frac{\varepsilon_{avg}}{\varepsilon_c}\right) \tag{31}$$

The area A_i then becomes

$$A_i = \frac{\pi}{4} \left[D_1 + (D_2 - D_1) \left(\frac{\varepsilon_{avg}}{\varepsilon_c}\right) \right]^2 \tag{32}$$

A compaction strain ε_c of 0.50 in./in. appears reasonable for the rigid polyurethane foam. Inserting this information into Equation (32) gives

$$A_i = \frac{\pi}{4}\left[D_1 + (D_2 - D_1)\left(\frac{\varepsilon_{avg}}{0.50}\right)\right]^2 \qquad (33)$$

For stresses above the yield stress of disc N = N

$$F = \sigma_N A_N \qquad (34)$$

Equations (14) and (16) can now be integrated in exactly the same manner given for the constant area case using Equation (26), (27), or (34) to determine the appropriate force F.

CHAPTER V

EXPERIMENTAL APPARATUS

IMPACT TESTING APPARATUS

The impact experiments were conducted using the apparatus illustrated schematically in Figures 14 and 15. Short - 1/2, 3/4 and 1-inch-long - cylindrical steel projectiles were accelerated to the impact velocity using a low-pressure air gun. The target, an 11-foot-long aluminum rod supported on Teflon mounts to allow free axial movement, was placed on axis with the gun barrel at the muzzle. The projectiles and the rod were nominally 1/2 inch in diameter. The mitigators were bonded to the impact end of the rod with a thin film of grease.

In order to obtain reasonable planarity between the impact faces of the projectile and the mitigator, the gun bore and the rod were aligned with the aid of a telescope. In addition, the impact was arranged to occur while the projectile was partially within the gun barrel. The driver gas was vented through holes in the barrel to eliminate the driving force from the projectile before the impact occurred. Thus, free-flight conditions existed in the axial direction at the time of impact.

Two light-sensitive transducers were placed one foot apart along the gun barrel near the muzzle to record the projectile transit time over that interval before impact. A small hole was drilled in the barrel at each location to allow light to impinge upon the transducer. As the projectile passed each location and the light beam was interrupted, each transducer generated an electrical signal. These signals were used to start and stop a Beckman/Berkeley Model 7260R time interval counter. The impact velocity was then determined from the relation

$$U_o = \frac{\Delta X}{\Delta T} = \frac{12 \text{ (inches)}}{\Delta T \text{ (seconds)}} \qquad (35)$$

A Hycam high-speed framing camera (5000 frames/sec.) was used to record the maximum strain of the mitigators. Although the entire time of contact between the projectile and the mitigator typically covers only 5 to 10 frames, the accuracy of the technique is reasonably good. Since the rate of change in strain is low at the time of maximum strain, the largest error encountered in the maximum strain measurement is less than 3 percent. The projectile rebound velocity was also determined from these films from the relation

$$U_r = \text{(distance/frame)} \cdot \text{(frames/second)} \qquad (36)$$

Strain gages were installed on the aluminum rod 12 inches from the impact end to record the force pulse transmitted by the mitigator. The gages were so installed and connected in a Wheatstone bridge as to cancel out the effect of bending. An excitation voltage of 6 volts was used to power the bridge. Prior to each test the bridge was balanced. During each test, the bridge imbalance was recorded on a Textronix-type 531 oscilloscope, fitted with a type-D plug-in unit and a type 123 preamplifier. The gain of the preamplifier was 100 to 1. The oscilloscope traces were recorded on Polaroid film and reduced to digital form using a telereader. For these particular test conditions, the 11-foot rod was of sufficient length to allow the transmitted pulse to completely pass the gage location before the leading edge of the pulse reflected from the free end of the rod arrived at the gage location. Hence, no analysis of the reflected pulse was necessary to unfold the transmitted pulse from the data.

COMPRESSION-TESTING APPARATUS

As input for the theoretical analysis, "quasi-static," medium strain rate and high-strain-rate stress-strain curves for the rigid polyurethane foam were experimentally determined in compression using a Baldwin-Southwark universal testing machine, a Plastechon Model 581 medium-strain-rate testing machine and a split Hopkinson pressure bar, respectively. The Baldwin-Southwark machine was a standard hydraulic-type machine with graphical load-deflection readout. The Plastechon Model 581 was simply a pneumatic-hydraulic version of the standard-type machine capable of higher crosshead speeds, but without servo control. This machine was not sufficiently rigid to measure strain via measuring crosshead displacement. Therefore, a pair of matched Optron Model 680AX electro-optical trackers were used to measure the strain by tracking the displacements of the two faces of the specimens. The tracker outputs were recorded on an oscilloscope equipped with a differential amplifier. The load was simultaneously recorded on the second channel of the same oscilloscope. The oscilloscope traces were photographically recorded,

converted to digital form with the aid of a telereader and combined to form the stress-strain curves. The corresponding strain rate was determined from the slope of the strain-time data.

The split Hopkinson pressure bar was used to obtain stress-strain data at strain rates on the order of 1000 in./in./sec. The basic concepts which govern the use of the split Hopkinson pressure bar are found in References 9 and 10. The material specimen is placed between two elastic bars. A compressive stress wave is propagated along one bar to the bar specimen interface. This stress wave is partially reflected and partially transmitted through the specimen into the second bar. Taking compressive strains as positive, the average strain rate in the specimen is related to the reflected strain in the first bar as follows:

$$\dot{\varepsilon}_s = \frac{-2g}{L} \varepsilon_r \tag{37}$$

where g is the wave velocity in the bar and L is the initial length of the specimen. The specimen strain may be determined by the integration of the above relation.

$$\varepsilon_s = \frac{-2g}{L} \int_0^T \varepsilon_r \, dt \tag{38}$$

The average specimen stress is related to the transmitted strain as follows:

$$\sigma_s = E \left(\frac{A_b}{A_s} \right) \varepsilon_T \tag{39}$$

where E is the Young's modulus of the bar material and A_b/A_s is the area ratio of the bar to the specimen.

The split Hopkinson pressure bar experiments were performed at the same facility as the impact experiments. The long rod was replaced by the two steel pressure bars. The short projectiles were replaced by a 10-inch-long projectile to produce an appropriate stress wave.

CHAPTER VI

EXPERIMENTAL AND THEORETICAL RESULTS

Prior to conducting each experiment, the dimensions, mass and density of the mitigator to be tested were determined. During each experiment, the following quantities were measured:

1. Projectile impact velocity
2. Projectile rebound velocity
3. Maximum mitigator strain
4. Transmitted force as function of time

Following each experiment, the initial projectile energy and the energy absorbed by the mitigator were calculated. These data are presented in Table 2.

Typical data records of the strain in the rod are shown in Figure 16 for nominally 18.5 lbs./ft.^{3} cylindrical and conical foam mitigators impacted at approximately 410 in./sec. by a 0.05-pound projectile. Since the rod remains elastic at all times, the strain in the rod is directly proportional to the force transmitted by the mitigator. Therefore, these strain-time data can be viewed as force-time data. The curves are characterized by steep, but finite rises, slowly decreasing or increasing plateaus, and gradual decays. For the cylindrical mitigator, the force decreases slightly along the plateau due to the strain rate effect. For the conical mitigator, the effect due to the area change is sufficient to offset the effect due to strain rate. The continual increase in stress area causes the force to increase slightly along the plateau.

The critical test of the model is its ability to match the transmitted force pulse measured in the experiments. Energy and velocity comparisons are less sensitive to the details of the modeling. Figure 17 illustrates the application of the three models to the case of the 0.05-pound projectile impacting a 3/8-inch-diameter by 3/8-inch-long, 18.5 lbs./ft.^{3} foam cylindrical mitigator at 410 in./sec. Clearly, the RPL model does not predict a realistic force pulse. The rise time is infinitesimal, the plateau is flat, and the delay time is infinitesimal. The addition of elasticity in the EPC model introduces a finite rise time and somewhat longer decay time in the calculated force pulse. Except for the flat plateau, this force pulse resembles the experimental data very closely. Adding the strain-rate-dependent plateau stress in the EPRC model produces the decreasing force along the plateau seen in the experimental data.

Similarly, Figure 18 illustrates the application of the three models to the case of the 0.05-pound projectile impacting a 3/8-inch-diameter by 1/2-inch-diameter by 3/8-inch-long, 18.5 lbs./ft.^{3} foam, conical mitigator at 410 in./sec. The results are similar to those obtained for the cylindrical mitigator except for the increasing force along the plateau. It is interesting to note that because of the competing area and strain rate effects, the EPRC model does not predict the peak force to occur at maximum strain. It will be seen later that this result agrees well with the experimental data.

TABLE 2

TEST CONDITIONS AND DATA

TEST NO.	MITIGATOR						PROJECTILE			ENERGY		
	ρ	L	D_1	D_2	$\epsilon_{MAX_{exp}}$	$\epsilon_{MAX_{theo}}$	WT.	U_o	U_r	KE_{proj}	$E_{A_{exp}}$	$E_{A_{theo}}$
	lbs/ft^3	in.	in.	in.	in/in	in/in	lbs.	in/sec	in/sec	in-lbs	in-lbs	in-lbs
1	18.3	.375	.375	*	19.1	19.3	.0505	411	98	11.1	9.6	10.1
2	18.9	.374	.378	.505	16.7	15.8	.0505	405	95	10.7	8.9	9.4
3	10.7	.378	.375	*	53.2	48.4	.0505	421	44	11.6	-	-
4	10.9	.378	.367	.494	38.3	37.3	.0505	418	67	11.4	10.7	10.9
5	10.9	.503	.376	*	44.4	35.5	.0505	418	58	11.4	-	-
6	11.0	.502	.374	.497	31.3	29.5	.0505	421	65	11.6	10.9	11.0
7	10.9	.502	.376	*	9.5	10.5	.0505	208	73	2.8	2.3	2.6
8	10.8	.502	.372	.492	9.5	10.4	.0505	211	60	2.9	2.5	2.7
9	10.9	.378	.382	.500	12.5	12.0	.0505	210	56	2.9	2.5	2.6
10	10.9	.377	.368	.490	36.2	31.8	.0379	433	75	9.2	8.6	8.8
11	11.0	.378	.372	.493	25.0	20.9	.0249	417	78	5.6	5.2	5.3
12	10.8	.377	.372	.498	-	58.2	.0505	618	-	25.0	-	22.2

* D_2 omitted for cylindrical mitigators

Although the EPRC model produces the most representative transmitted force-time curve, a dip develops in the calculated curve as the projectile comes to rest and begins to rebound. The dip is not evident in the experimental data. At this point in the calculation, the strain rate is decreasing very rapidly and the predicted strain-rate dependence of the plateau stress is excessive. Since the dynamic material property data were obtained under constant strain-rate conditions, and constant strain-rate conditions do not exist under impact loading, these data are not expected to apply in every detail. More information is needed on the time dependence of the mechanical properties of foam materials.

Furthermore, the logarithmic function fitted to the stress-strain rate density data (Equation (3))

$$\sigma = (C_1 + C_2 \ln \dot{\varepsilon}) \rho^{K_1}$$

becomes undefined at zero strain rate. The problem is averted in the calculation simply by allowing the time step to bridge the zero strain-rate point. Other investigators, for example, Perrone, have used a different function

$$\sigma = \sigma_o \left[1 + \left(\frac{\dot{\varepsilon}}{C_3} \right)^{\frac{1}{K_2}} \right] \qquad (40)$$

to describe the strain-rate dependence without encountering the above problem. Instead the problem becomes that of determining σ_o. As applied to foam materials, the authors do not believe that σ_o is statically determinable. To avoid the aforementioned dip in the force-time curve, the value of σ_o must be greater than that determined statically. Unless the proper dynamic σ_o is obtained, Equation (40) offers no improvement over Equation (3).

Theoretical results, corresponding to the experiments, were obtained using the computer program listed in Appendix B. Impact velocity, projectile mass, foam density and mitigator length were varied to test the flexibility of the EPRC model. Maximum mitigator strain and energy absorption are given in Table 2 for comparison.

The experimental and theoretical transmitted force-time curves of test 1 are presented in Figure 19. These results are for an 18.3 lbs./ft.^{3} cylindrical mitigator. The experimental curve shows considerably more structure than the theoretical analog. The initial peak may be caused by the tendency of this material to peak at yield and then drop rapidly to some plateau stress at the high strain rate. Subsequent oscillations are due more to electronic noise than to material response. In general, the theory matches the experiment well with slight differences in amplitude and pulse length.

Similar curves for test 2 are shown in Figure 20. These results are for an 18.9 lbs./ft.^{3} conical mitigator subjected to nearly the same impact conditions as those of test 1. The agreement between experiment and theory is excellent, except for a small difference in amplitude. Note that the peak in the theoretical curve, which occurs before the mitigator reaches maximum strain, parallels the experimental data quite well.

Tests similar to tests 1 and 2 were performed on nominally 10.8 lbs./ft.^{3} foam mitigators to determine the effect of mitigator density on the transmitted force-time curve and energy absorption. The curves for tests 3 and 4 are given in Figures 21 and 22, respectively. Somewhat poorer agreement in amplitude between theory and experiment is encountered. The magnitude of the transmitted force is about 40 percent of that transmitted by an 18.6 lbs./ft.^{3} foam mitigator. The pulse length, on the other hand, is more than doubled.

Tests 5 and 6 were performed under the same impact conditions. The mitigators used in these tests were of the same nominal density as those of tests 3 and 4, but were 30 percent longer. The transmitted force-time curves for these tests are shown in Figures 23 and 24. The results are not significantly different, except for smaller maximum strains, Table 2.

For tests 7 and 8 the impact velocity was reduced to 210 ft./sec. All other aspects of these tests remained similar to those of tests 5 and 6. The resulting force-time curves are presented in Figures 25 and 26. The rise times of the pulses have been lengthened and the discrepancy between the experimental and theoretical results has increased. The pulse amplitudes are lower because of strain-rate effects and compare more favorably than those of tests 5 and 6. The pulse lengths are shorter and agreement is good between theory and experiment.

Returning to the use of a short mitigator, test 9 was performed in a similar fashion to test 8 with similar results, Figure 27. The theory predicts an increase in amplitude due to strain-rate effects with a corresponding reduction in the pulse length. However, the experimental data from tests 8 and 9 are virtually the same. Variations in material properties due to nonhomogeneity are probably sufficient to overshadow the predicted differences between these tests.

Tests 10 and 11 are similar to test 4 with the exception of a change in the projectile weight. For test 10, the weight was reduced by 25 percent and for test 11, the weight was reduced by 50 percent. Since the impact velocity is essentially the same, the kinetic energies of the projectiles are proportional to their relative weights. And, since the force developed upon impact is essentially the same, the major effect of reducing the projectile weight is to shorten the pulse length, Figures 28 and 29.

The experimental force-time curve for test 12 is presented in Figure 30. The impact velocity for this test was increased to 618 in./sec. For this projectile velocity, the mitigator should have compacted. However, the foam material crumbled or exploded due to the air trapped within the voids. This explains why no large increase in force due to compaction is seen in the data. At low strain rates, the foam would have simply crushed. Apparently, the maximum amount of energy that a rigid foam mitigator can absorb without self-destructing is dependent upon strain rate, decreasing with increasing rate.

CHAPTER VII

CONCLUSIONS

The experimental data and the theoretical results contained in this report permit the following conclusions regarding the validity of the material model and the effectiveness of rigid polyurethane foam as a shock mitigator.

1. The elastic, perfectly plastic, strain-rate dependent compacting model adequately predicts the force transmitted by the mitigator as a function of time and the energy absorbed by the mitigator.

2. The elastic, perfectly plastic, strain-rate dependent compacting model is an improvement over the commonly used rigid, perfectly plastic locking model.

3. Mitigators of varying cross-sectional area are appropriately modeled.

4. More information is needed on the time dependency of the plateau stress of foams.

5. Rigid polyurethane foam is an effective shock-mitigating material, Figure 1, as long as compaction does not occur.

REFERENCES

1. Perrone, Nicholas, "On a Simplified Method for Solving Impulsively Loaded Structures of Rate-Sensitive Materials," Journal of Applied Mechanics, Vol. 32, Series E, No. 3, Sep 1965, pp 489-492

2. Green, S. J., Schierloh, F. L., Perkins, R. D., and Babcock, S. G., "High-Velocity Deformation Properties of Polyurethane Foams," Experimental Mechanics, Vol. 9, No. 3, Mar 1969, pp 103-109

3. Perrone, Nicholas, "A Mathematically Tractable Model of Strain-Hardening, Rate-Sensitive Plastic Flow," Journal of Applied Mechanics, Vol. 33, Series E, No. 1, Mar 1966, pp 210-211

4. Schmidt, W. and Hoffman, J., Verpackungs Rundschau, Technical Scientific Supplement - 16, Feb 1965

5. Mustin, Gordon S., Theory and Practice of Cushion Design, U. S. Department of Defense, The Shock and Vibration Information Center, Washington, D. C., for sale by the Government Printing Office, 1968, p 128

6. Schwaber, David M. and Meinecke, Eberhard A., "Energy Absorption in Polymeric Foams. II. Prediction of Impact Behavior from Instron Data for Foams with Rate-dependent Modulus," Journal of Applied Polymer Science, Vol. 15, No. 10, Oct 1971, pp 2381-2393

7. CPR Technical Information, CPR 18 Series, "Rigid Urethane Foam," The Upjohn Company, CPR Division, Torrance, California

8. Clark, Weldon Hawkins, Jr., "End Condition to Make a Bar Appear Infinitely Long to Stress Waves," Thesis, University of Maryland, College Park, Maryland, 1971

9. Rand, J. L., Yang, J. C. S., and Marshall, J. M., "Dynamic Compression Testing of a Strain-Rate Material," NOLTR 65-10, Oct 1965

10. Rand, J. L., "An Analysis of the Split Hopkinson Pressure Bar," Thesis, University of Maryland, College Park, Maryland, 1967

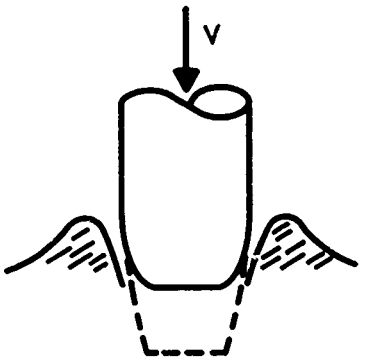

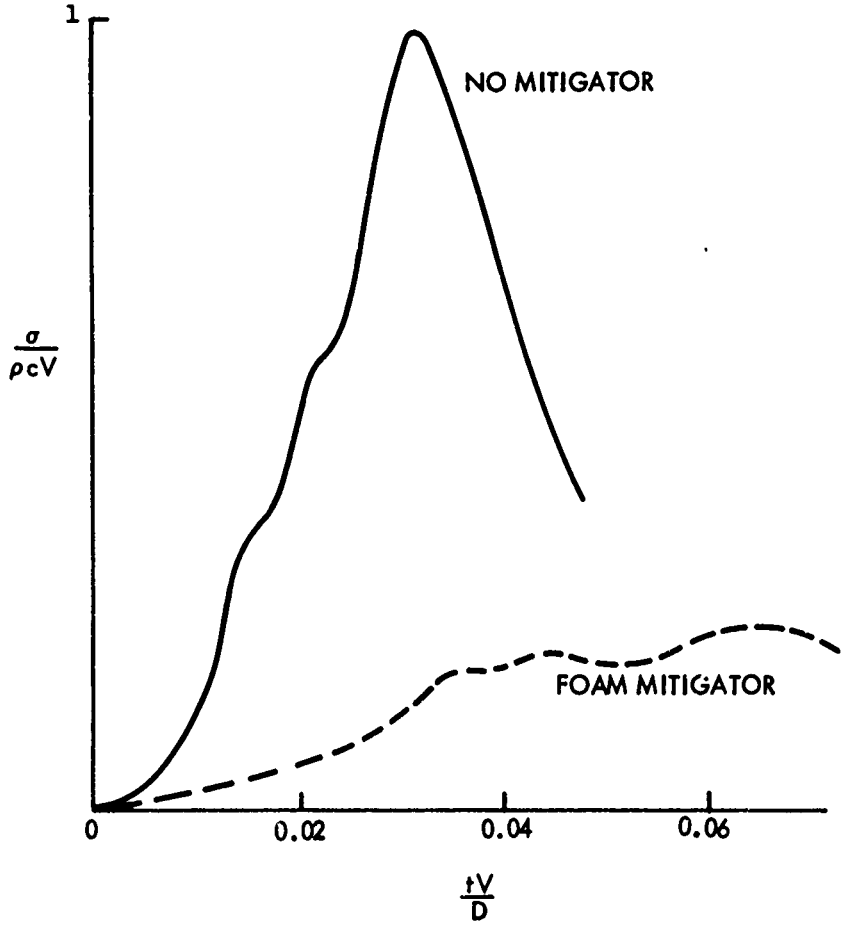

FIG. 1 STRESS PULSE AT NOSE OF TORPEDO-VERTICAL ENTRY

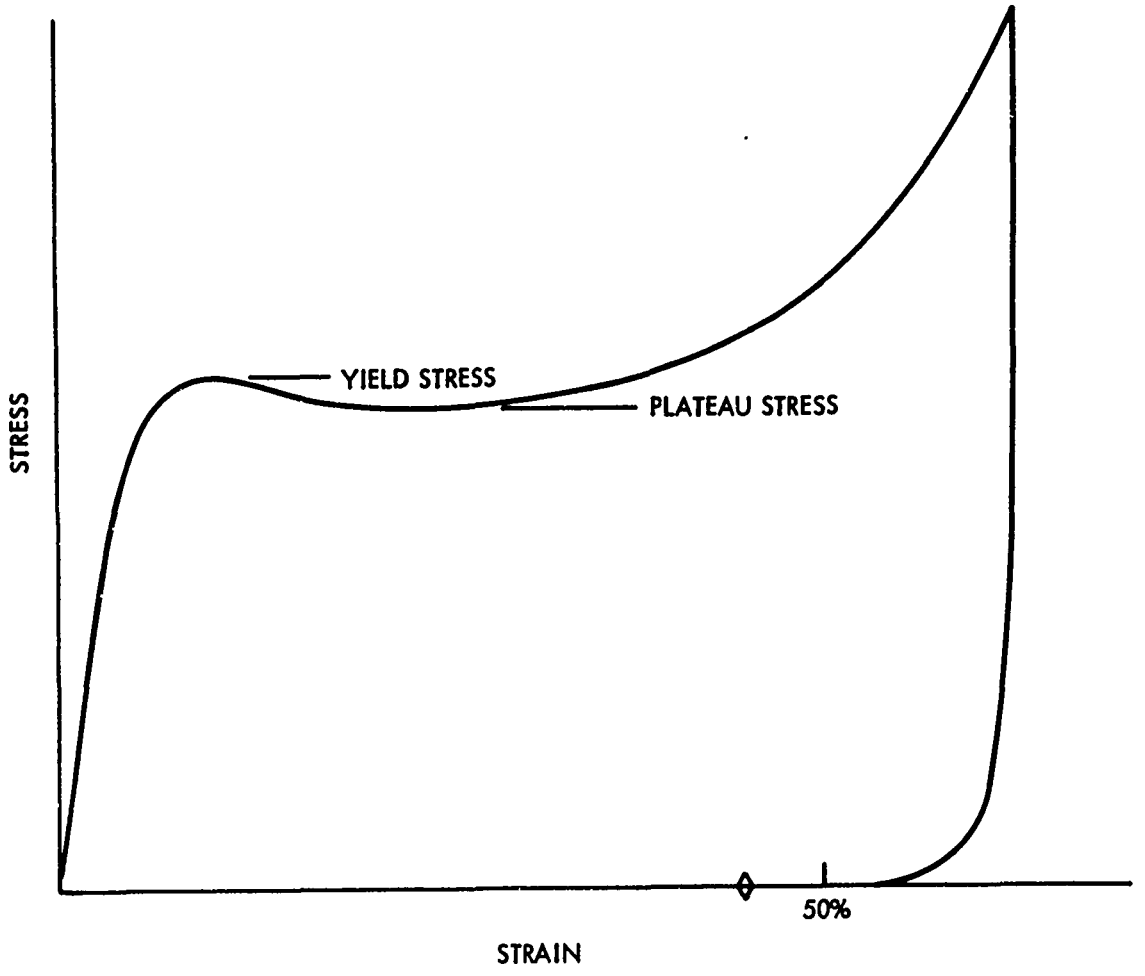

FIG. 2 TYPICAL STRESS-STRAIN CURVE FOR RIGID POLYURETHANE FOAM

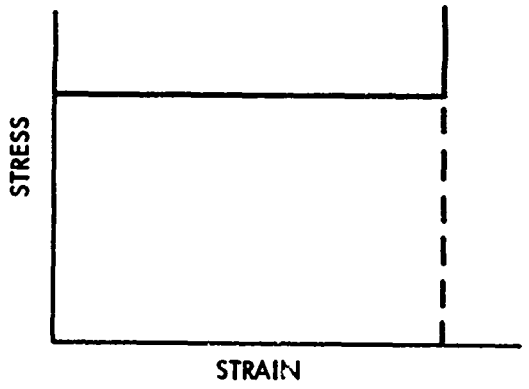

A-RIGID, PERFECTLY PLASTIC, LOCKING MODEL

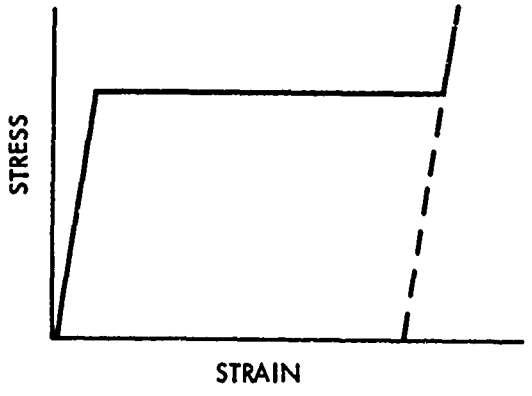

B-ELASTIC, PERFECTLY PLASTIC, COMPACTING MODEL

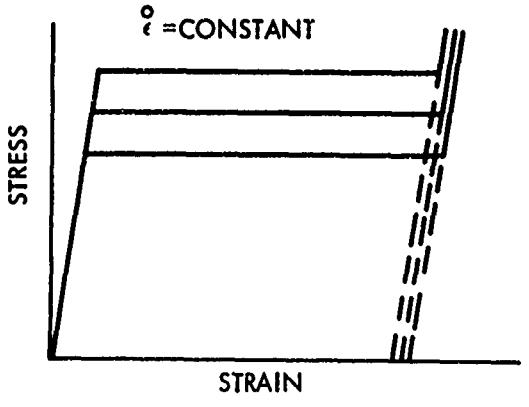

C-ELASTIC, PERFECTLY PLASTIC, STRAIN RATE DEPENDENT, COMPACTING MODEL

FIG. 3 MATERIAL MODELS

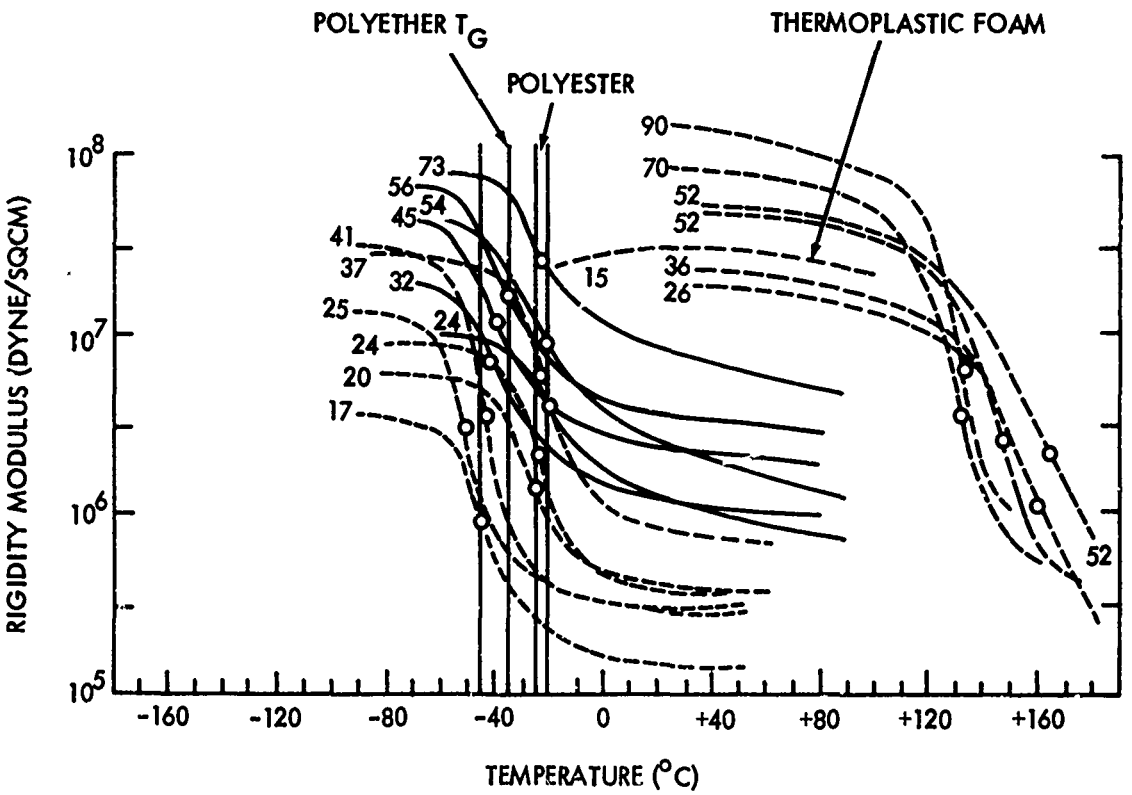

FIG. 4 RIGIDITY MODULUS FOR A NUMBER OF POLYURETHANE FOAMS *

*Taken from Reference 4

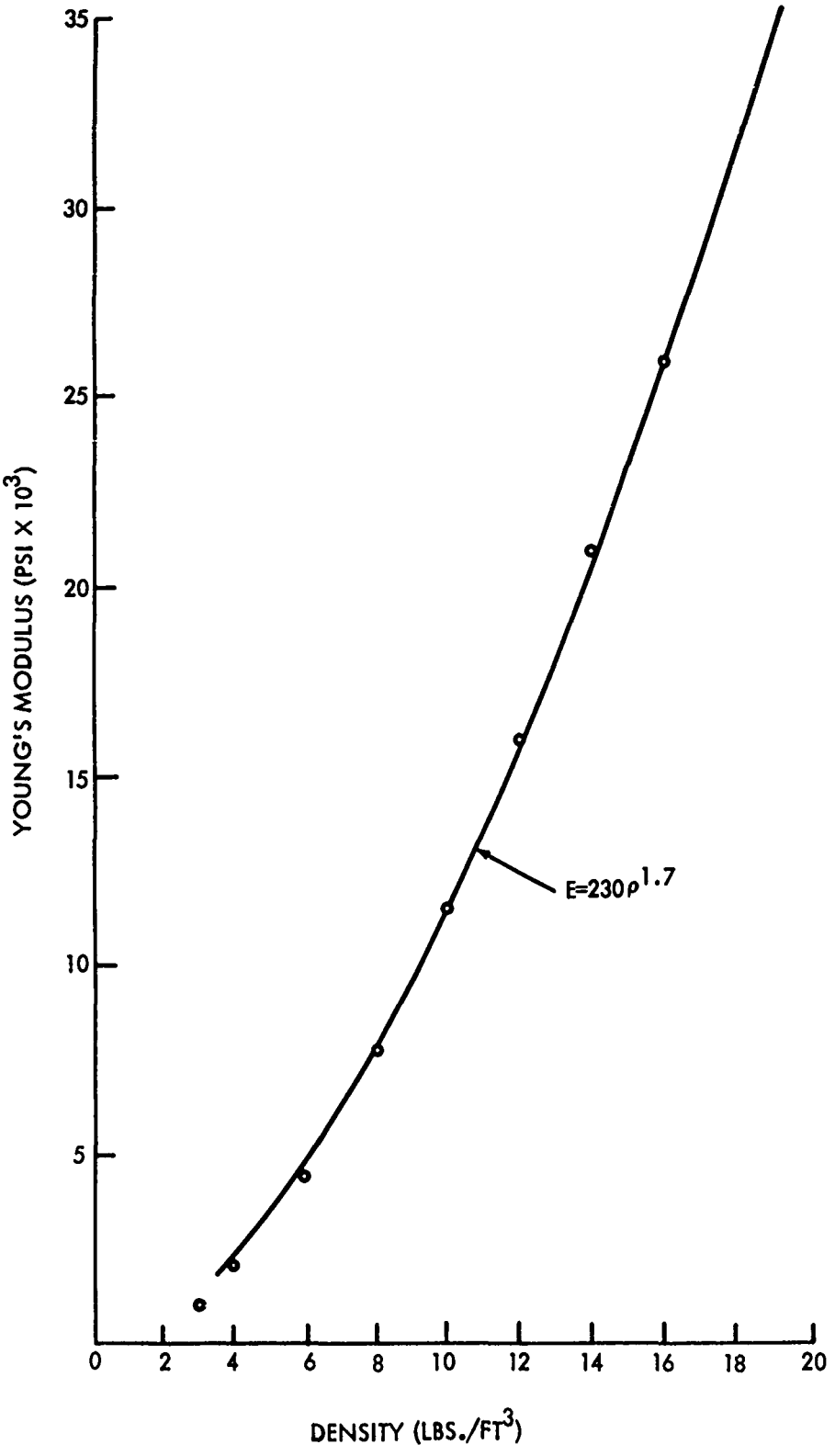

FIG. 5 CURVE FIT TO MODULUS - DENSITY DATA

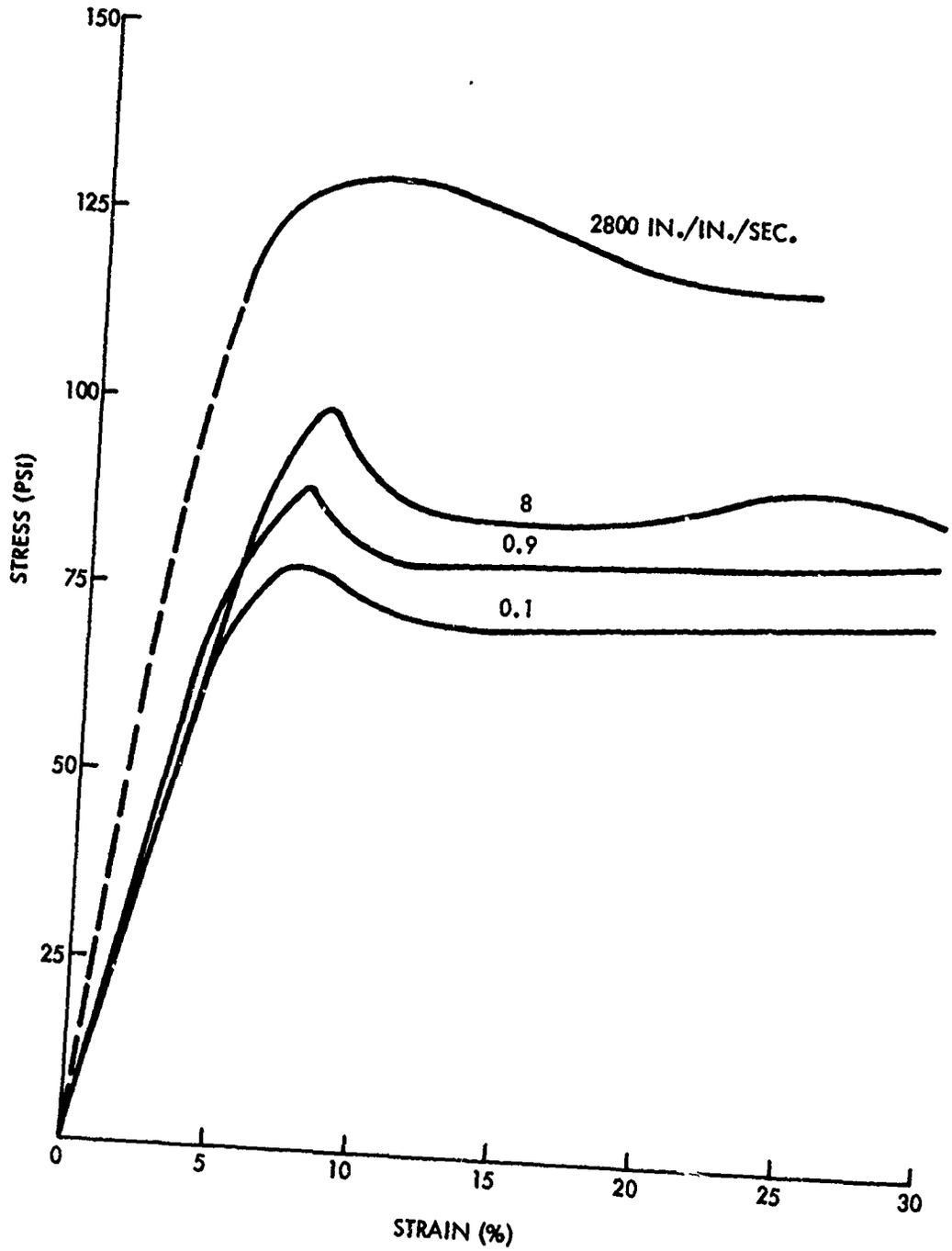

FIG. 6 TYPICAL STRESS-STRAIN CURVES FOR 3.5 LBS./FT^3 RIGID POLYURETHANE FOAM

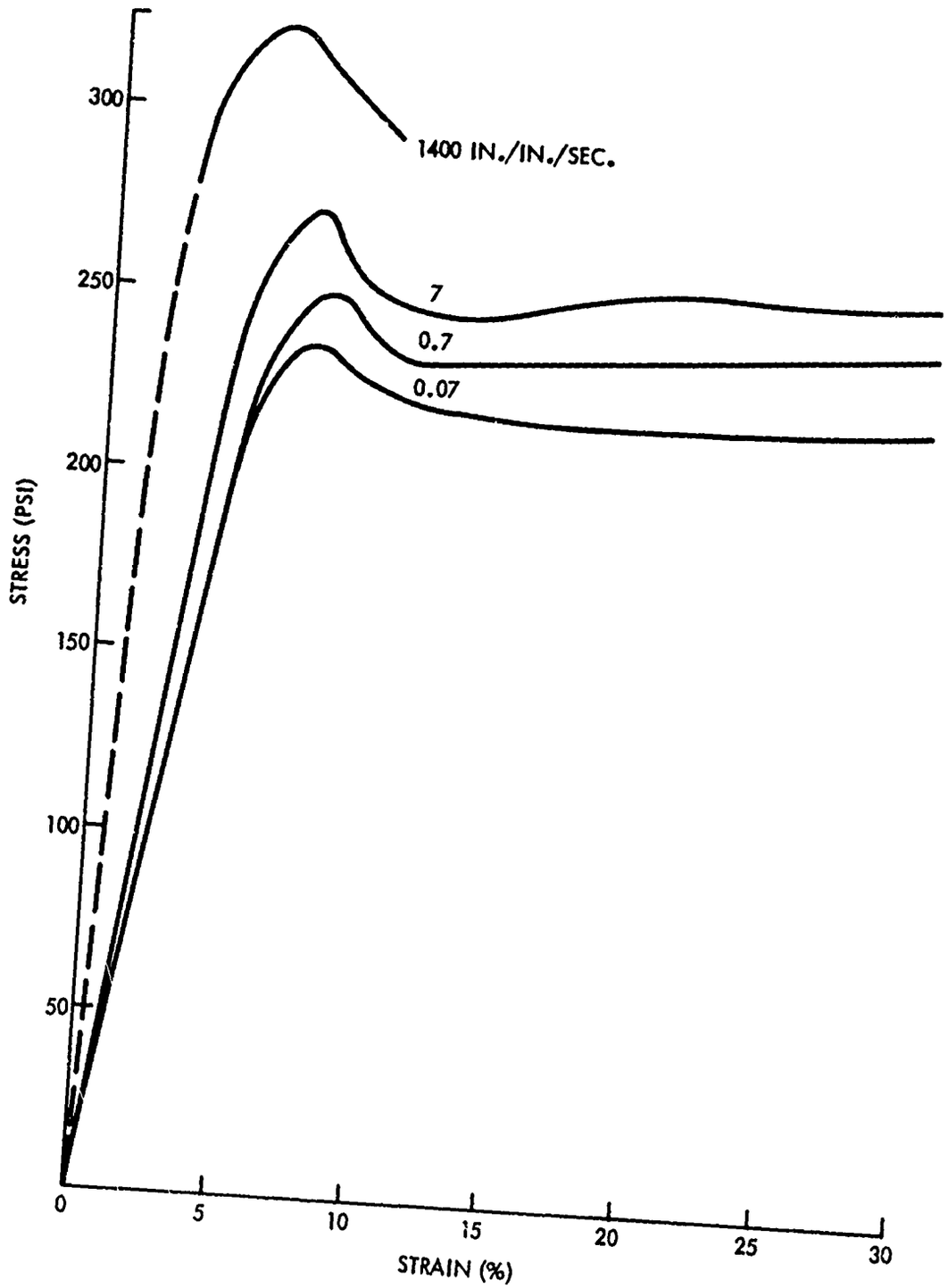

FIG. 7 TYPICAL STRESS-STRAIN CURVES FOR 7.0 LBS./FT.^{3} RIGID POLYURETHANE FOAM

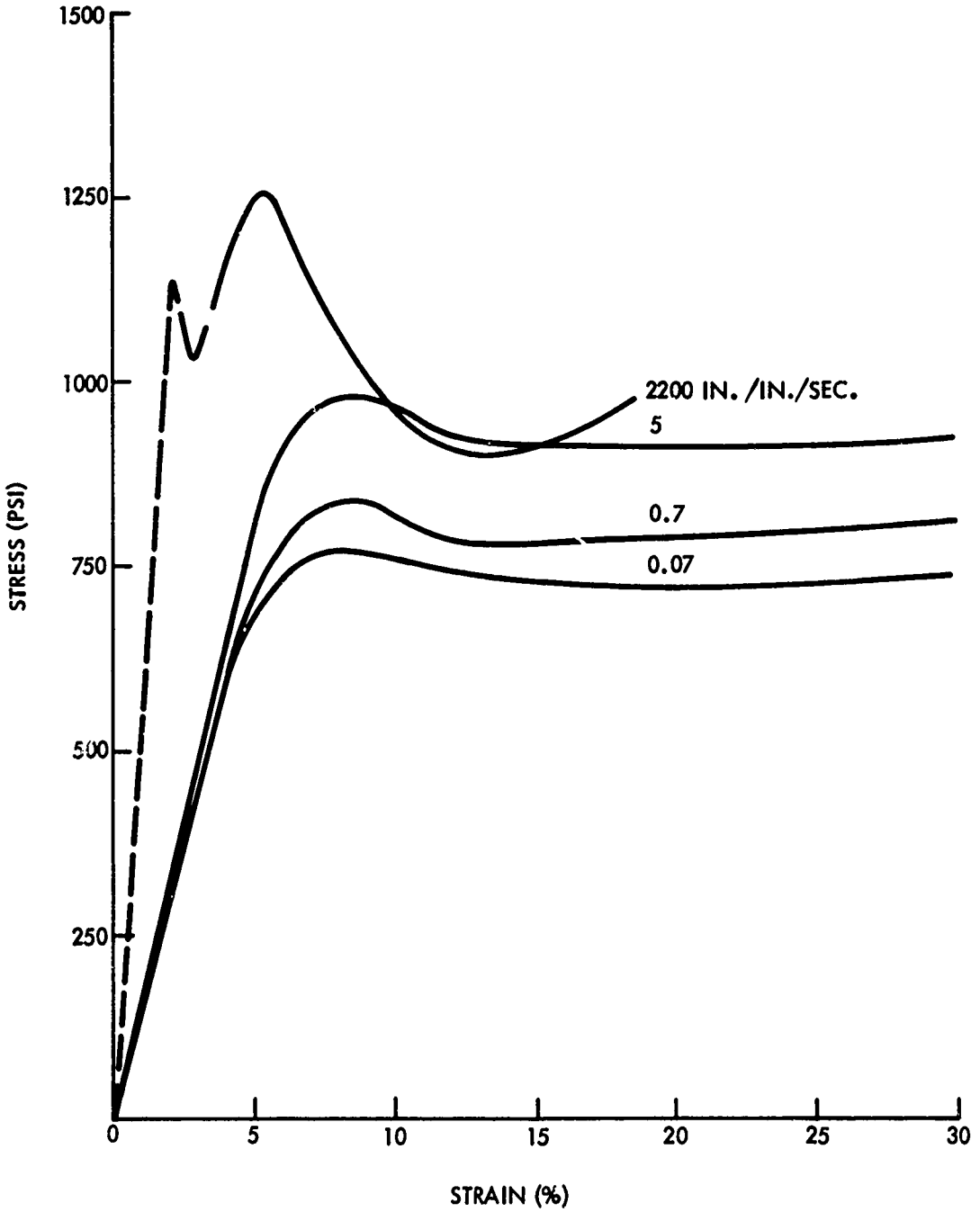

FIG. 8 TYPICAL STRESS-STRAIN CURVES FOR 14.5 LBS./FT.^{3} RIGID POLYURETHANE FOAM

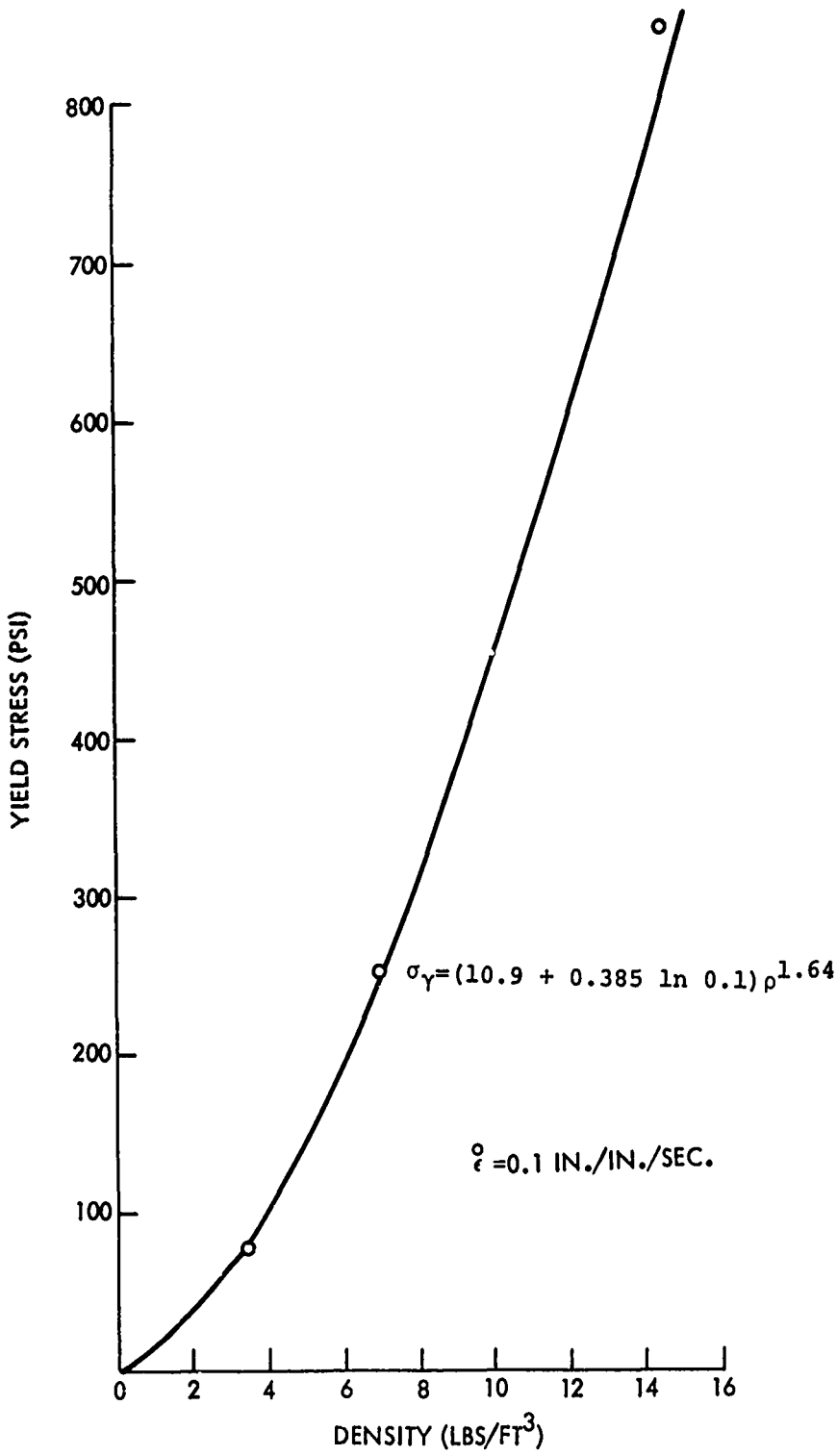

FIG. 9 DENSITY DEPENDENCE OF COMPRESSIVE YIELD STRENGTH OF RIGID POLYURETHANE FOAM

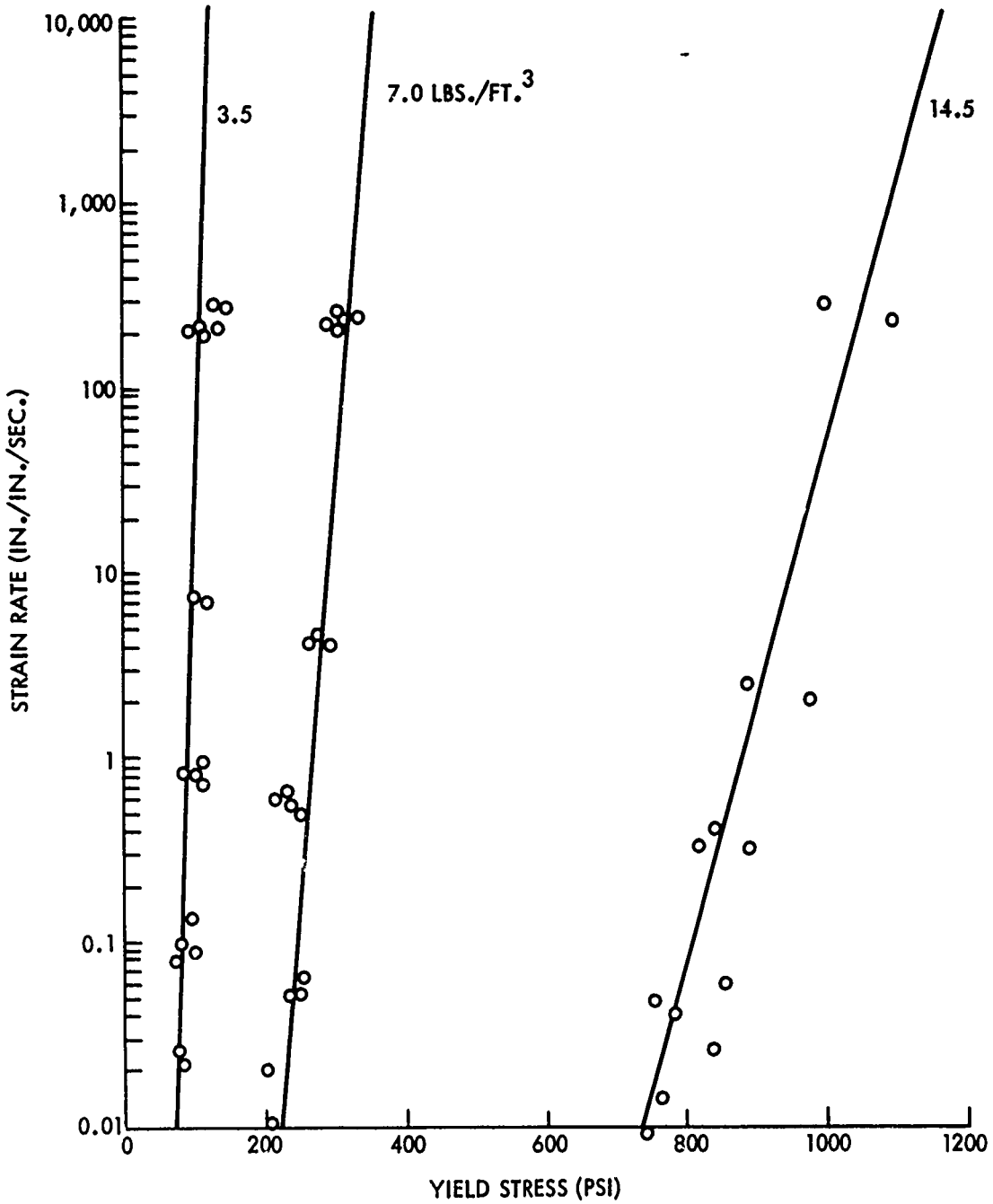

FIG. 10 STRAIN RATE DEPENDENCE OF COMPRESSIVE YIELD STRENGTH OF RIGID POLYURETHANE FOAM

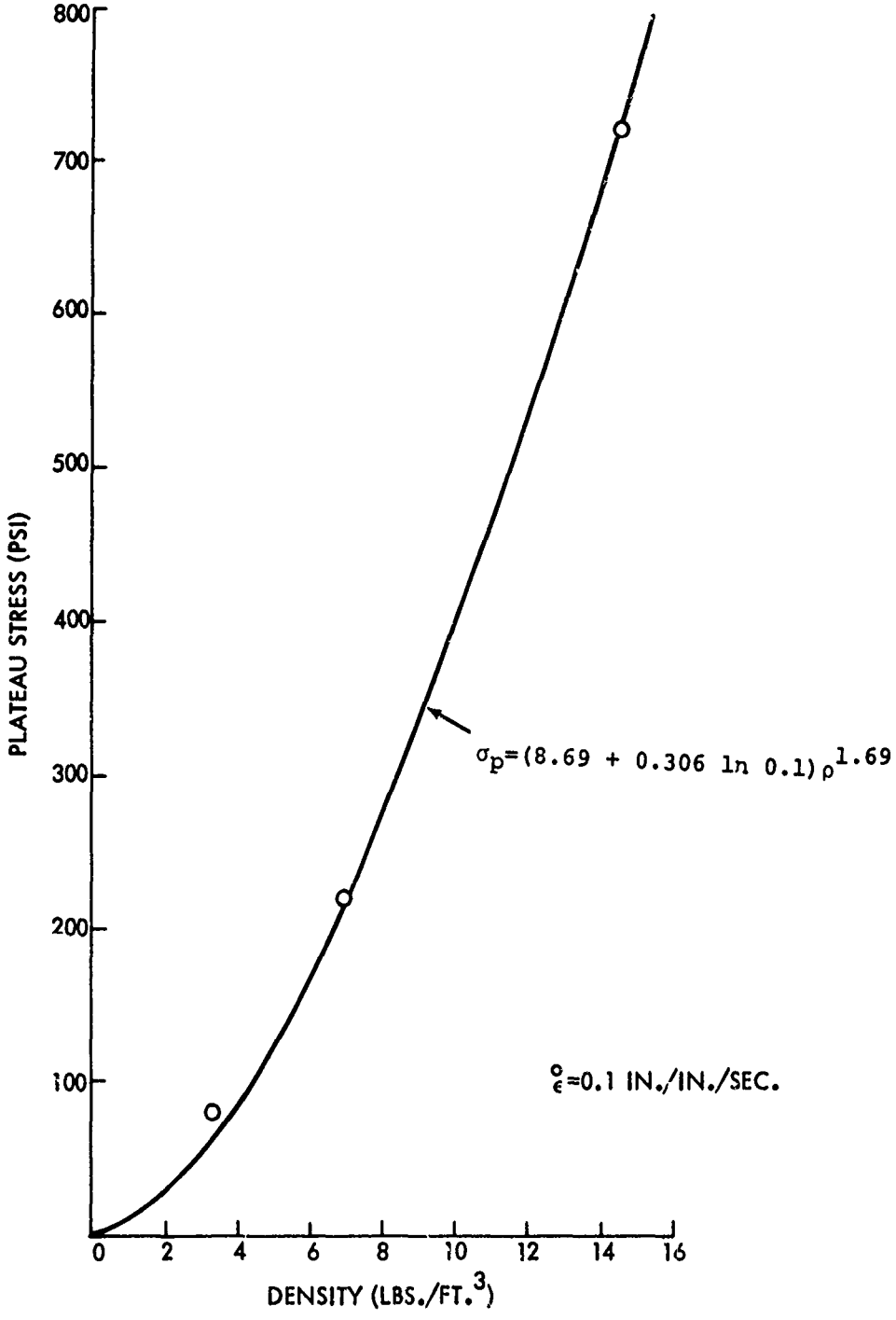

FIG. 11 DENSITY DEPENDENCE OF PLATEAU STRESS OF RIGID POLYURETHANE FOAM

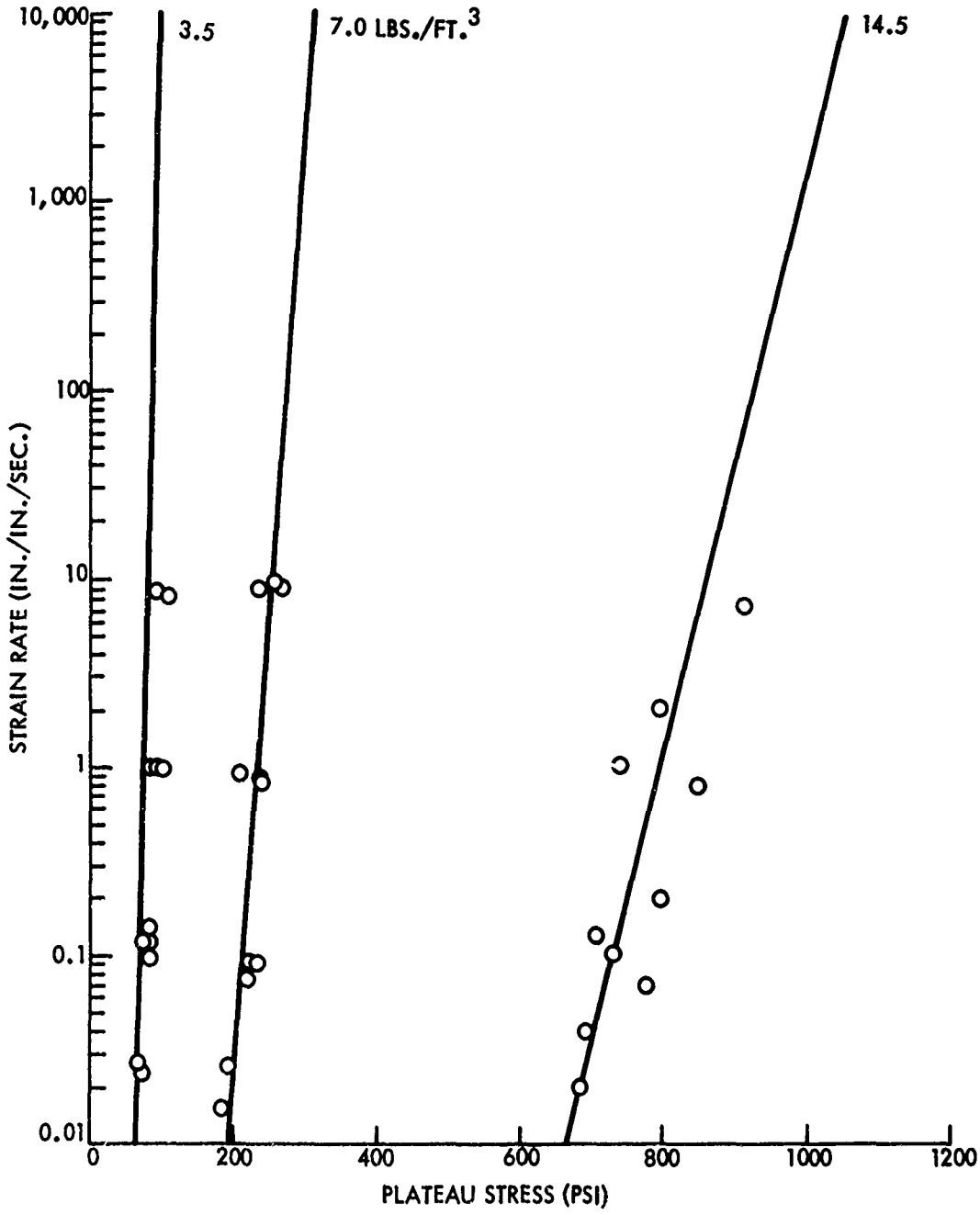

FIG. 12 STRAIN RATE DEPENDENCE OF PLATEAU STRESS OF RIGID POLYURETHANE FOAM

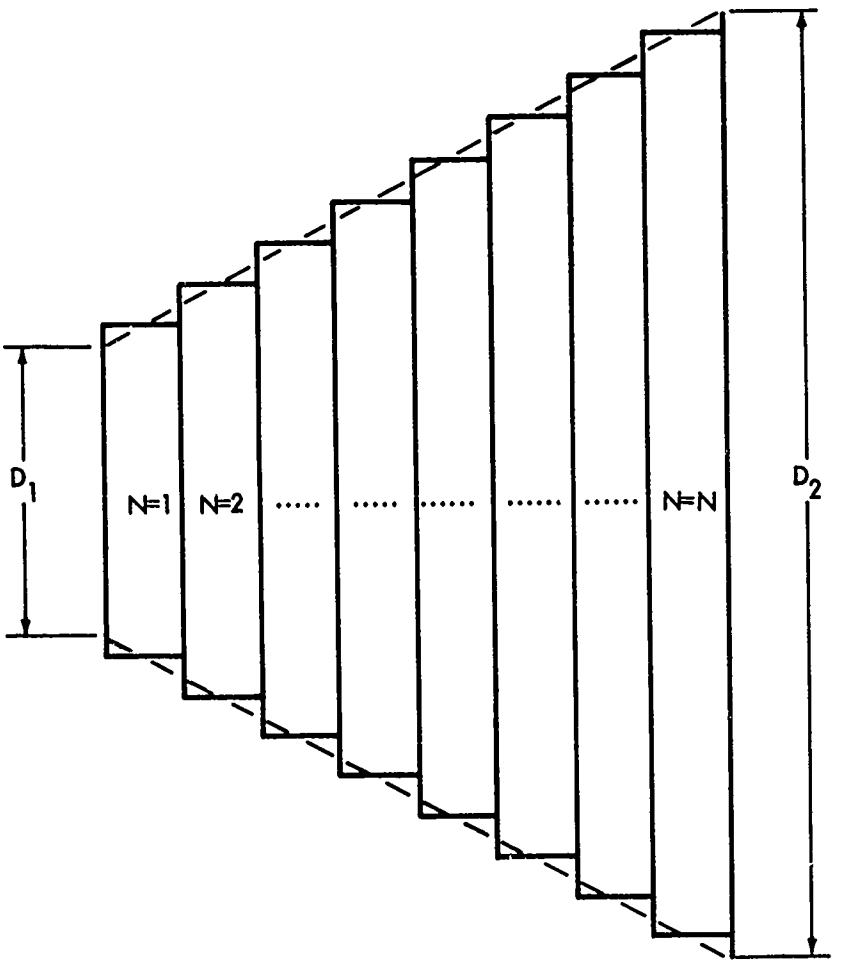

FIG. 13 VARYING AREA MITIGATOR

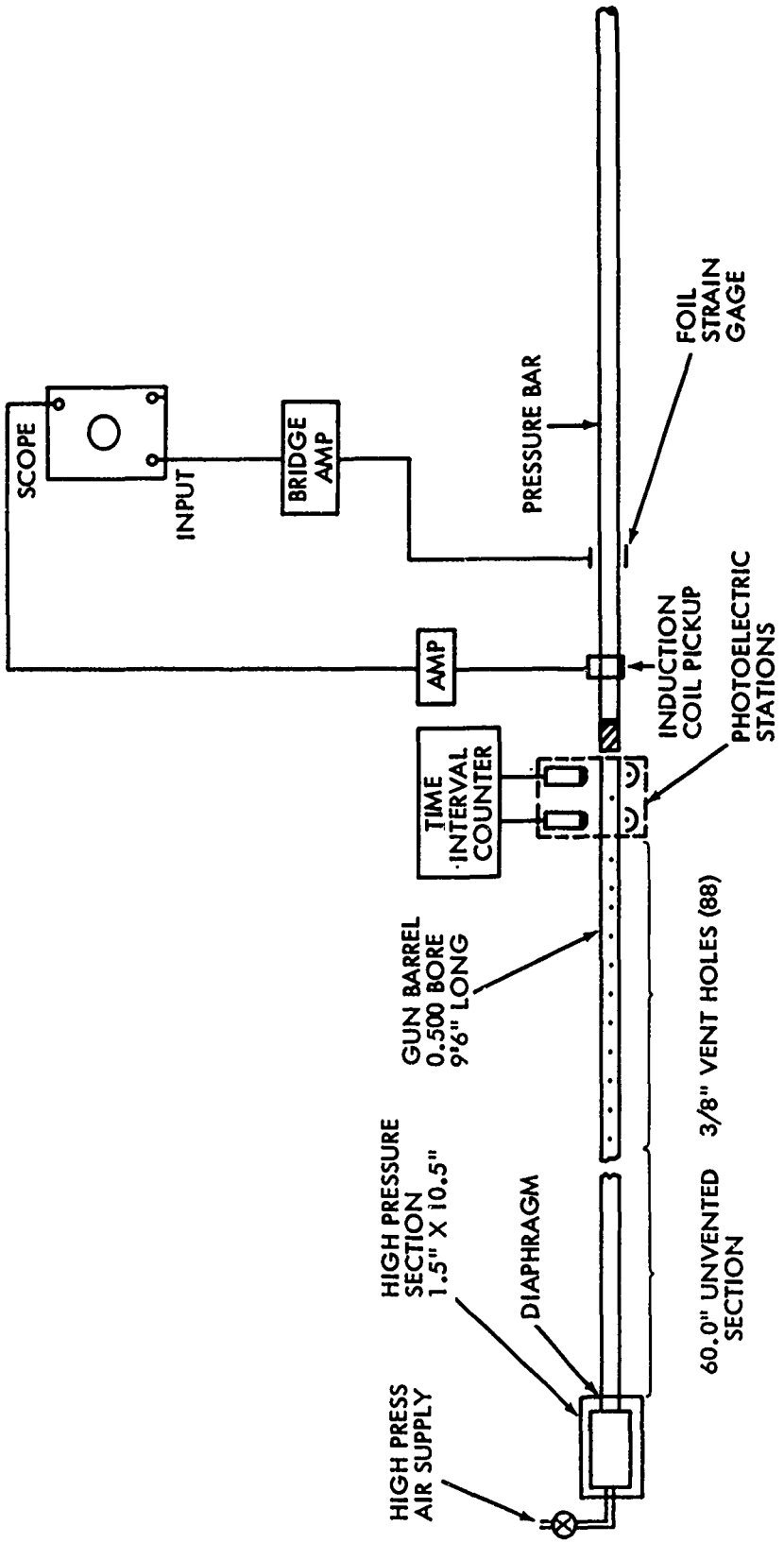

FIG. 14 SCHEMATIC OF TEST APPARATUS

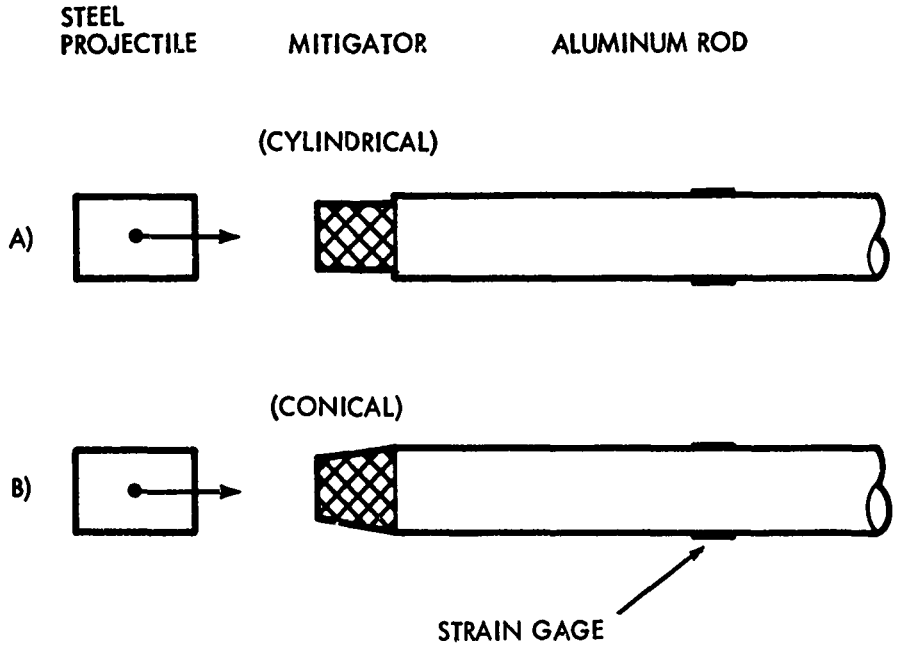

FIG. 15 IMPACT CONFIGURATIONS

(A) CYLINDRICAL MITIGATOR

(B) CONICAL MITIGATOR

FIG. 16 TYPICAL DATA RECORDS OF STRAIN IN ROD

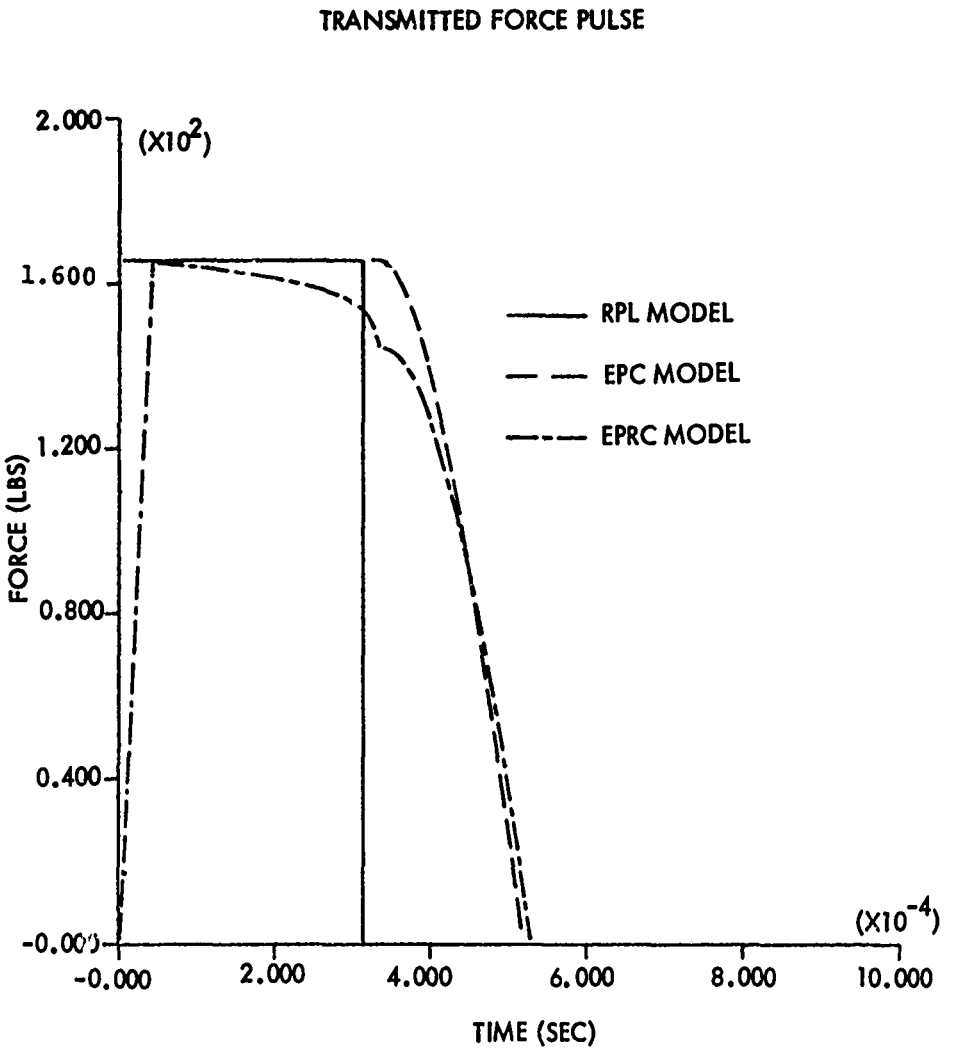

FIG. 17 TYPICAL THEORETICAL FORCE-TIME CURVES FOR CONSTANT AREA MITIGATORS

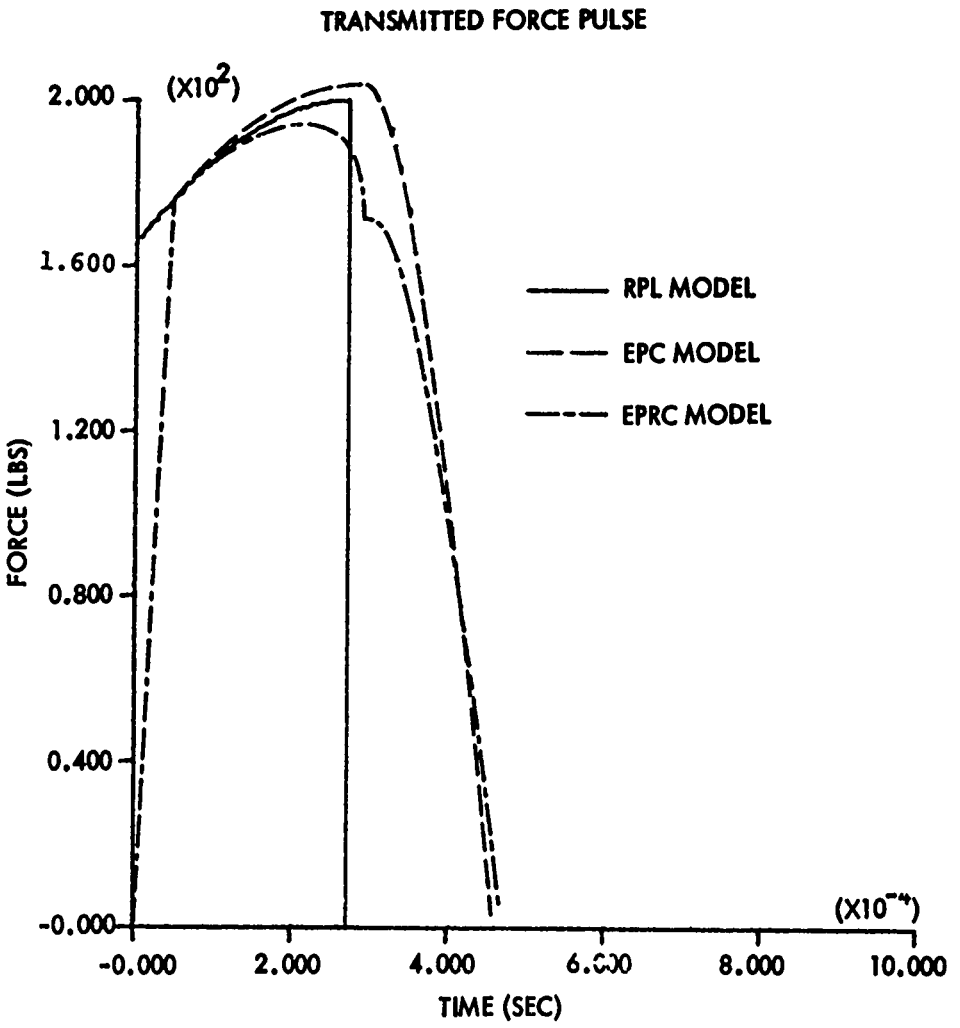

FIG. 18 TYPICAL THEORETICAL FORCE-TIME CURVES FOR VARYING AREA MITIGATORS

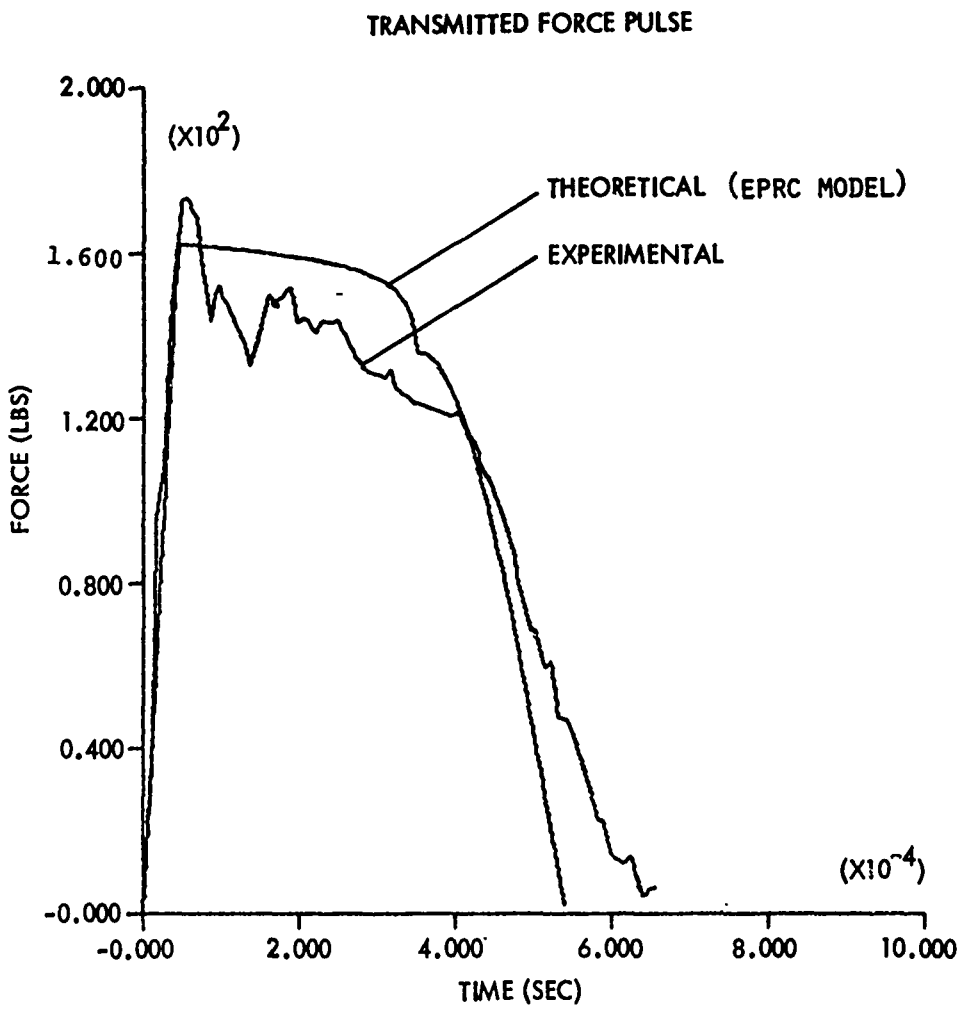

FIG. 19 TEST NO. 1

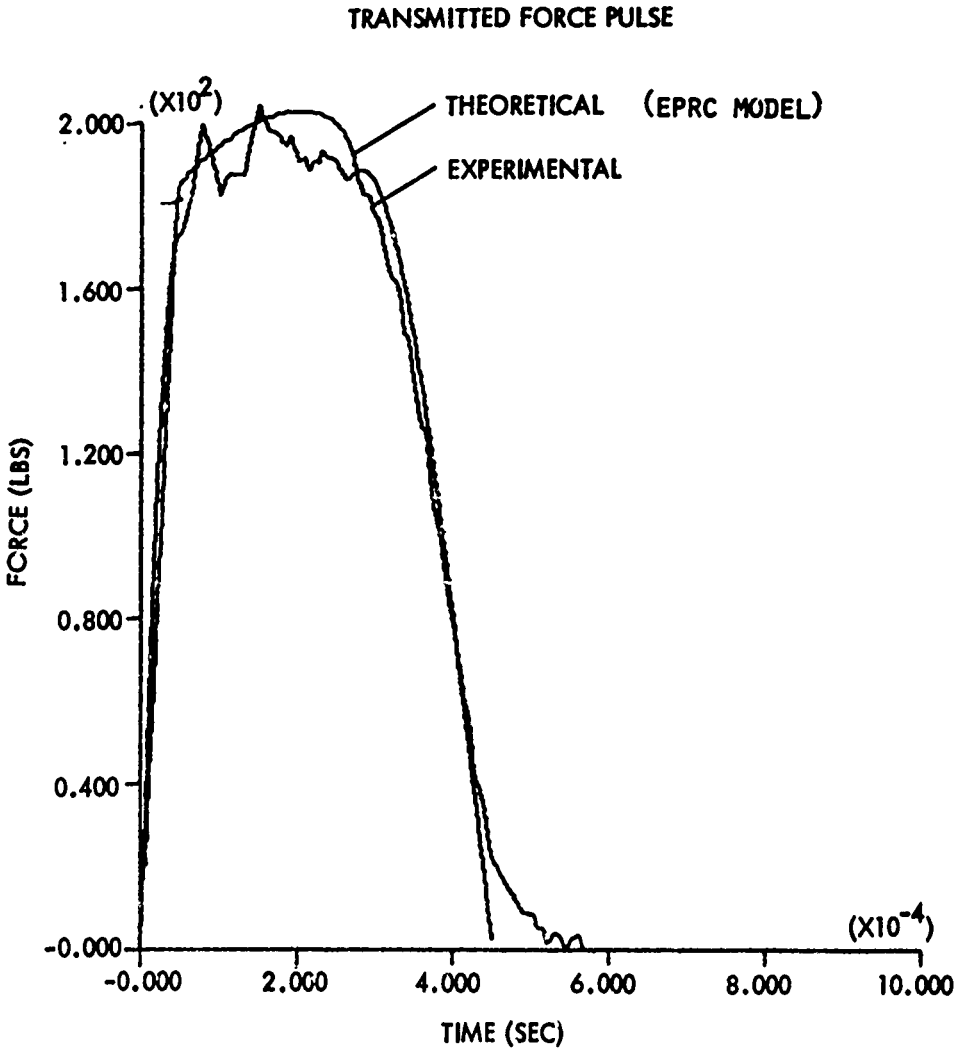

FIG. 20 TEST NO. 2

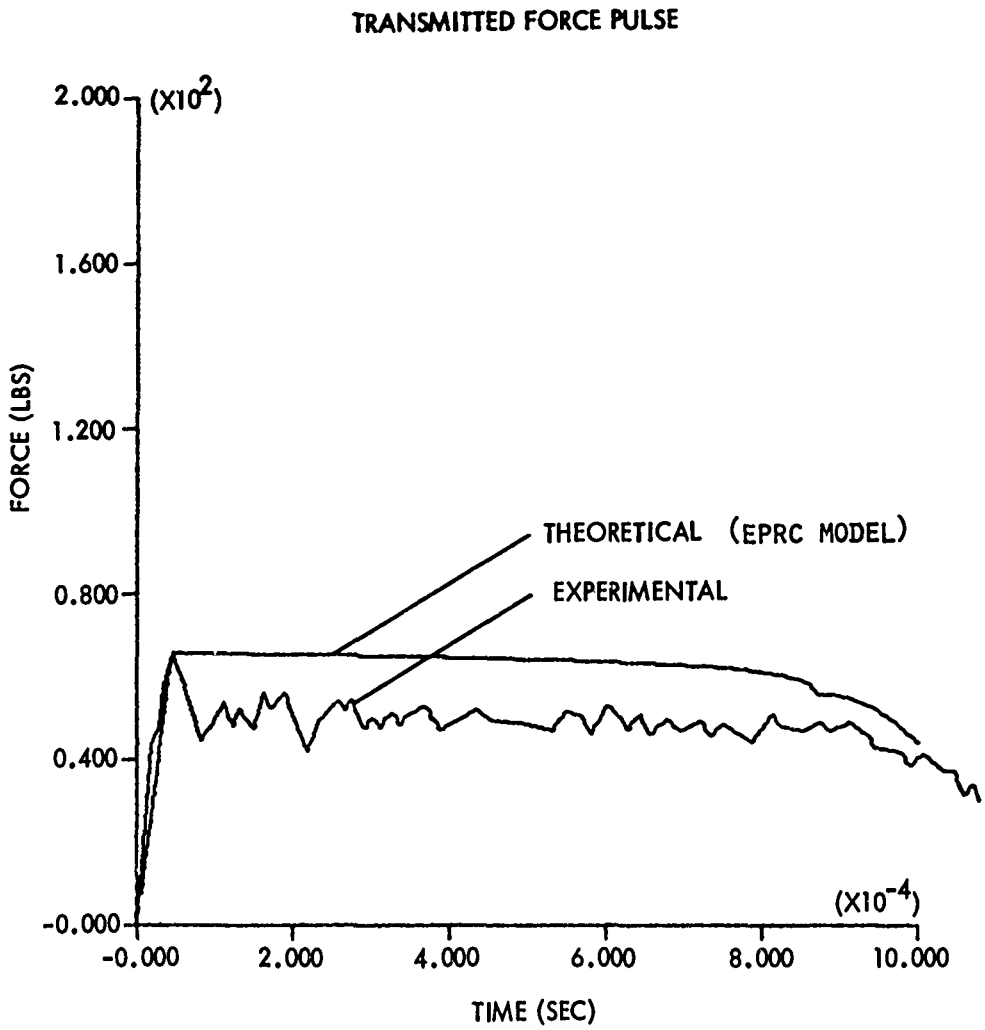

FIG. 21 TEST NO. 3

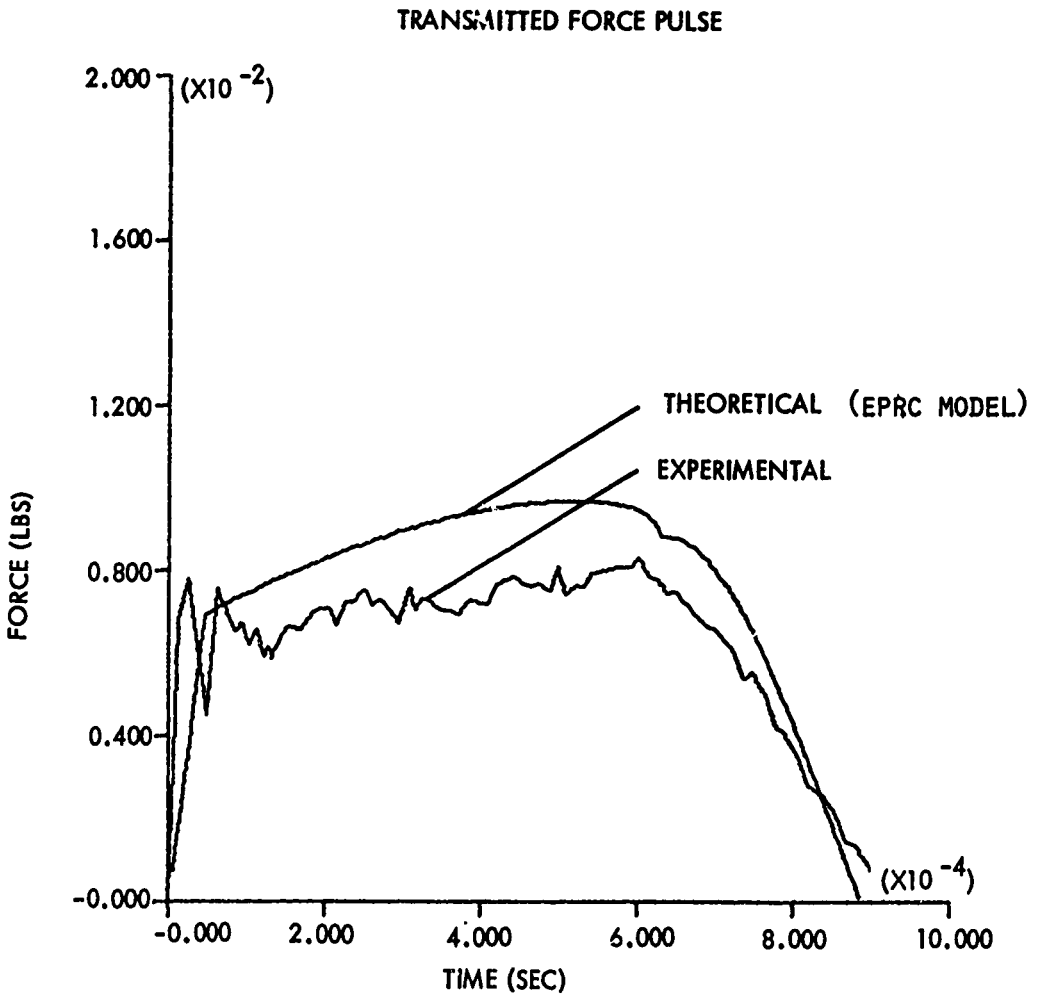

FIG. 22 TEST NO. 4

TRANSMITTED FORCE PULSE

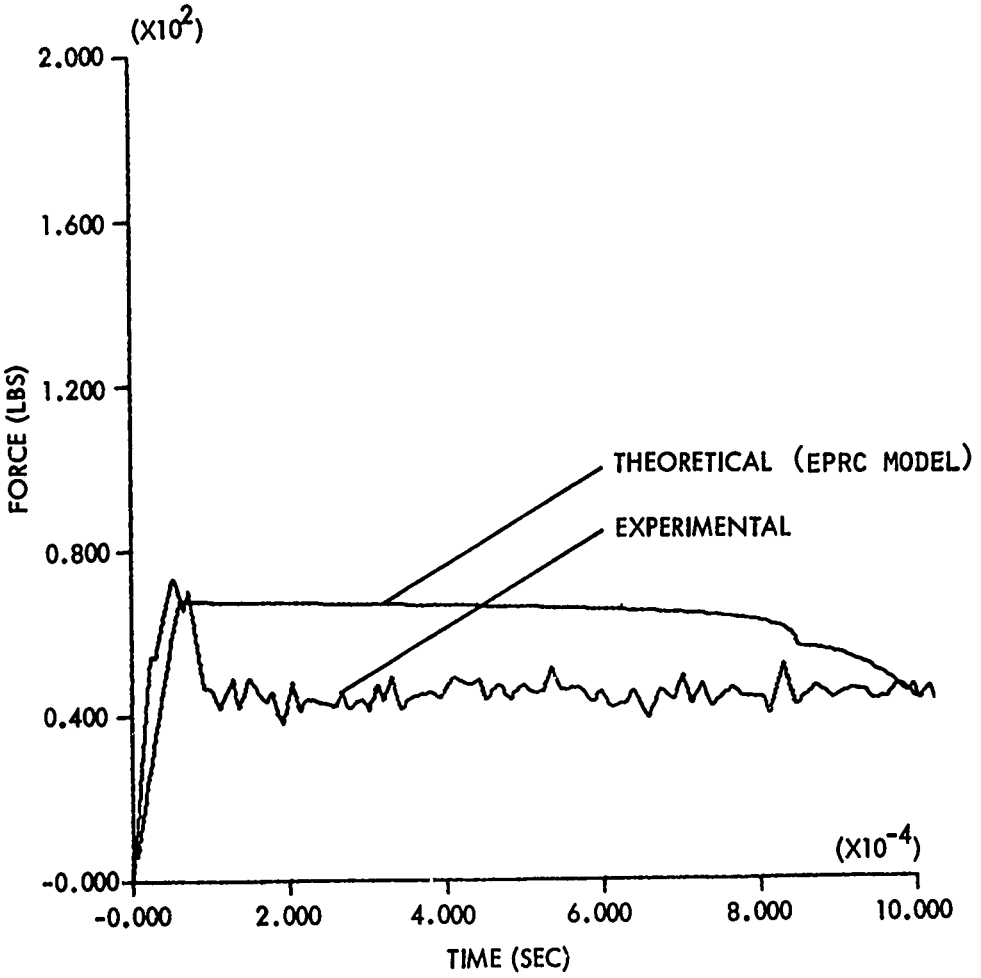

FIG. 23 TEST NO. 5

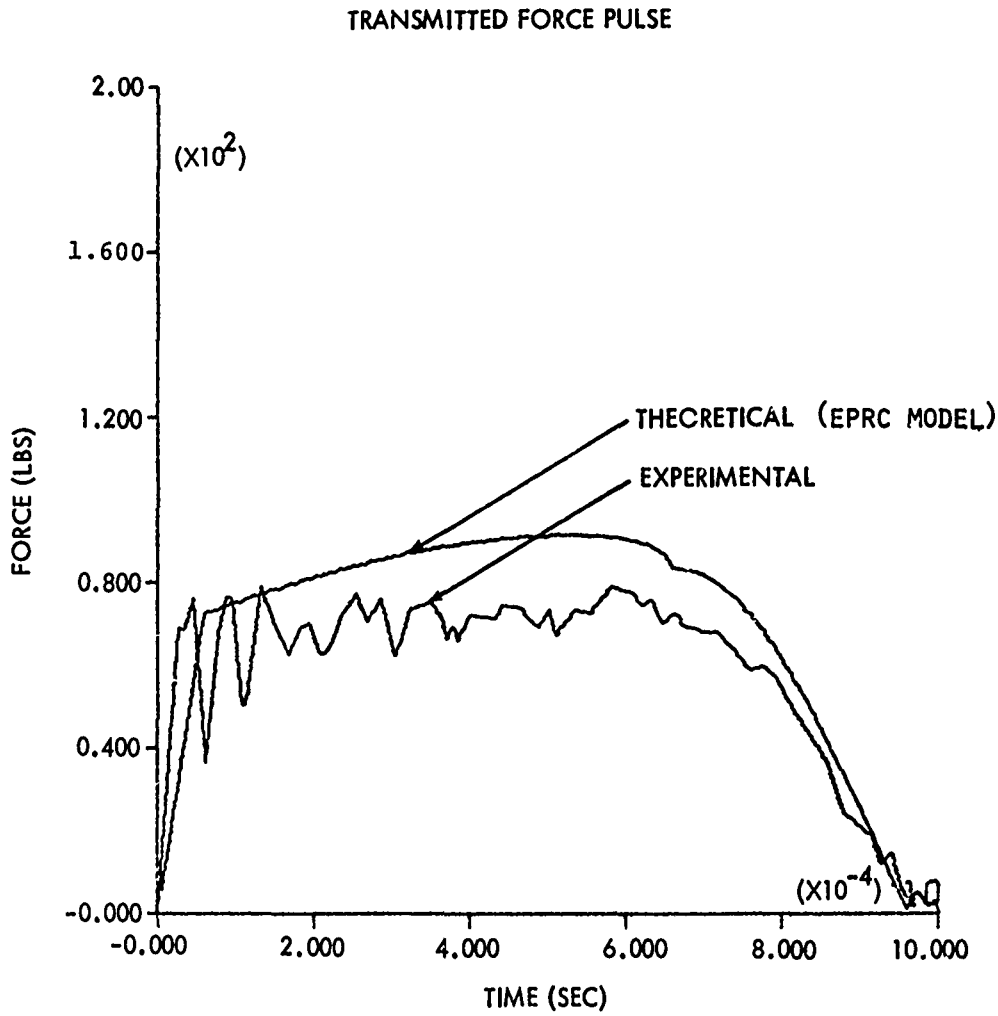

FIG. 24 TEST NO. 6

TRANSMITTED FORCE PULSE

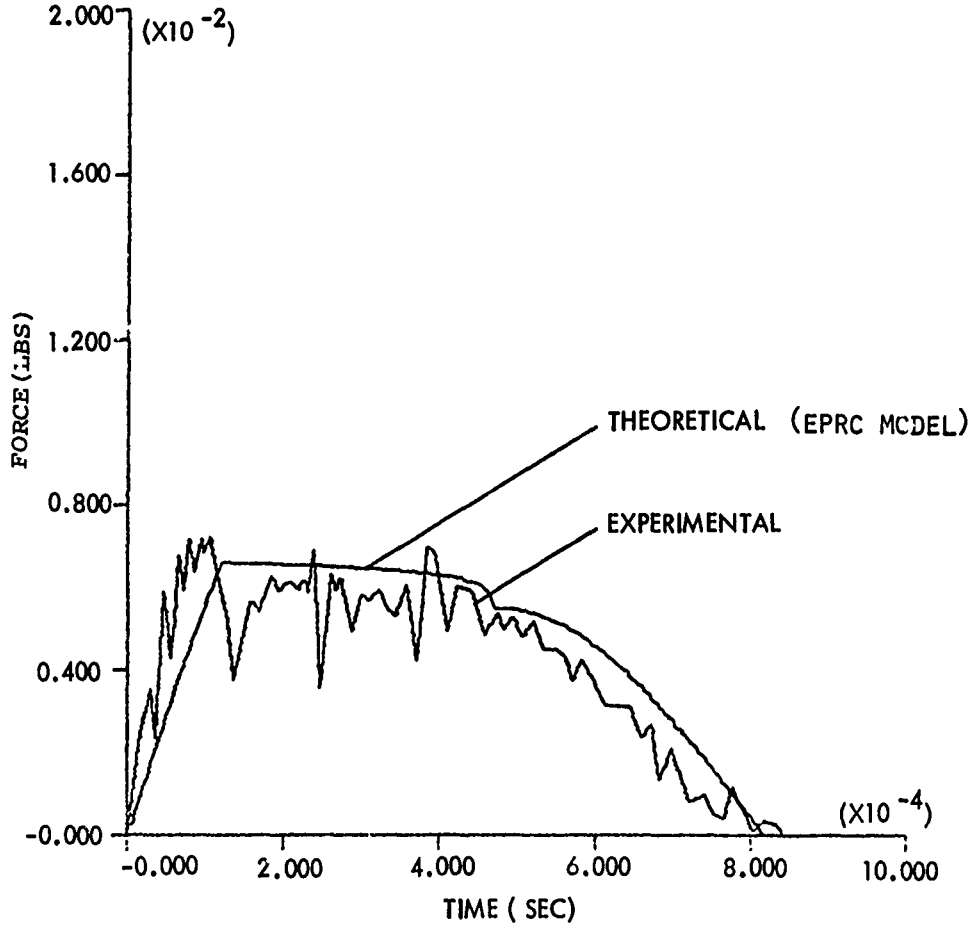

FIG. 25 TEST NO. 7

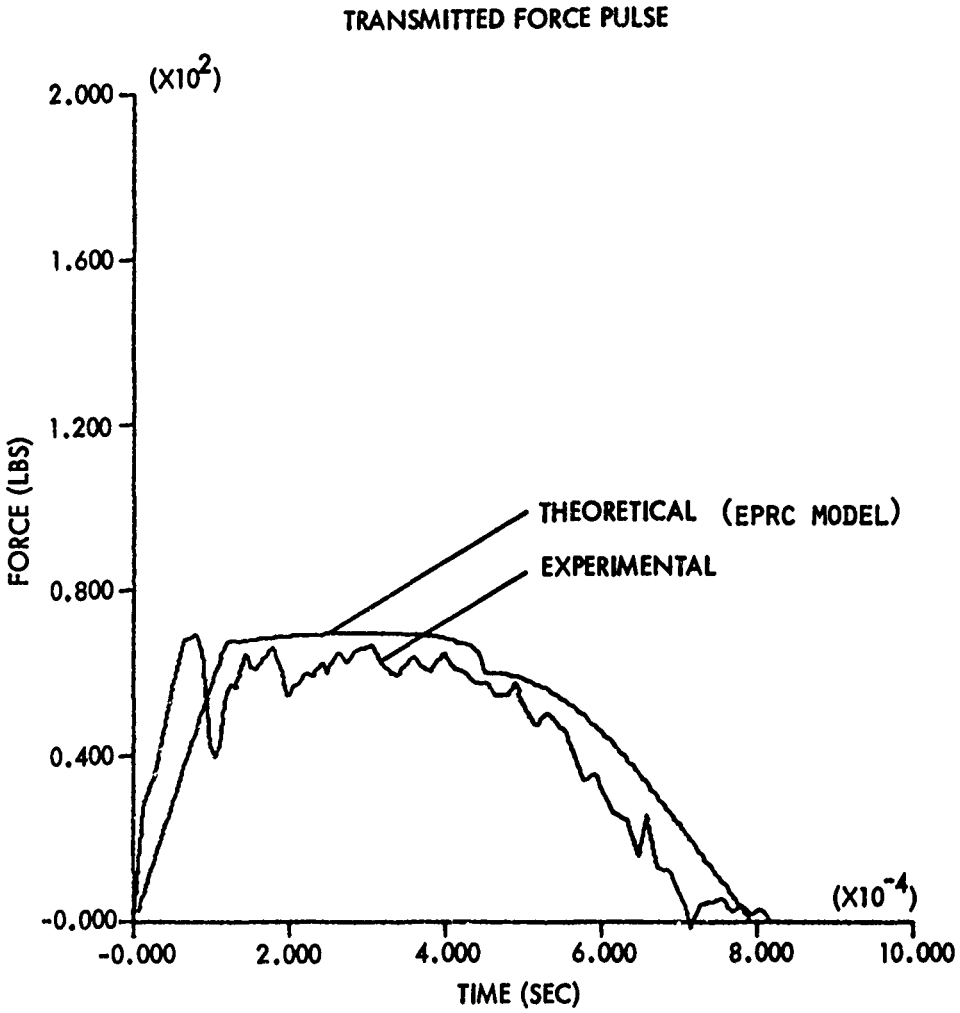

FIG. 26 TEST NO. 8

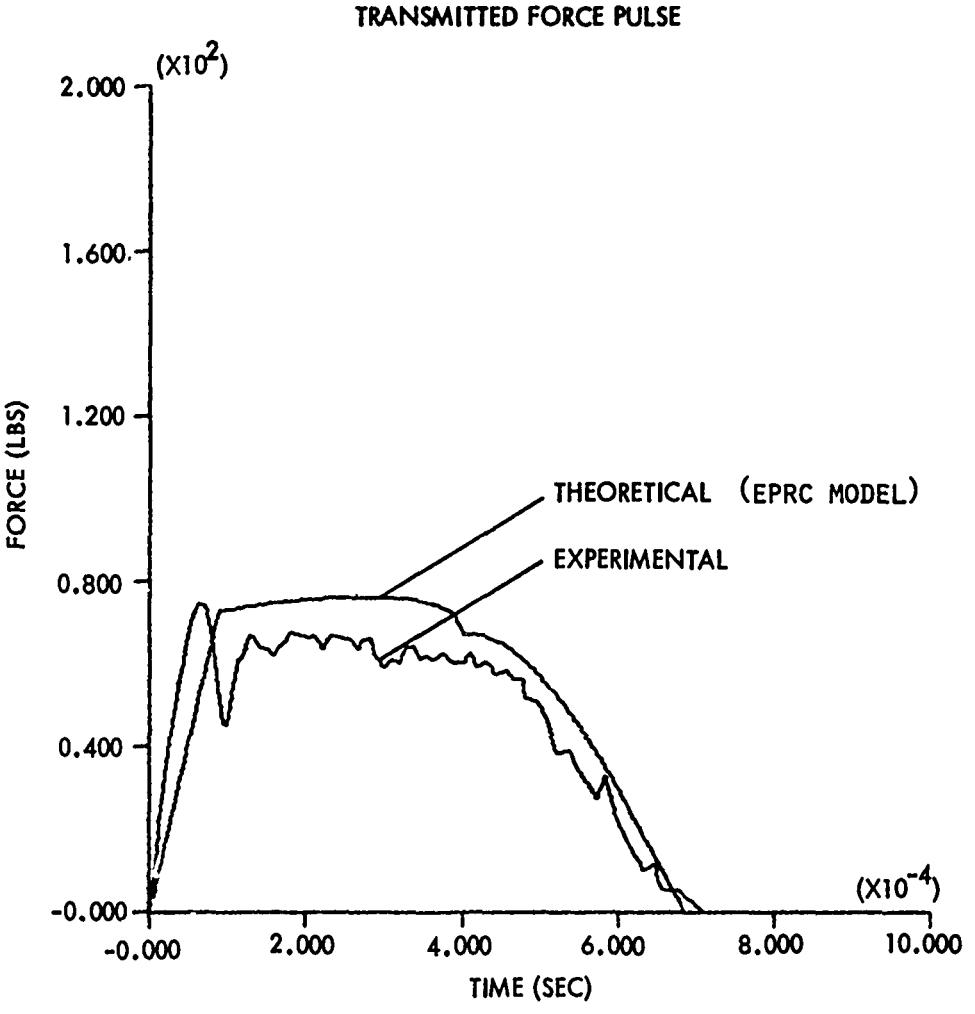

FIG. 27 TEST NO.9

TRANSMITTED FORCE PULSE

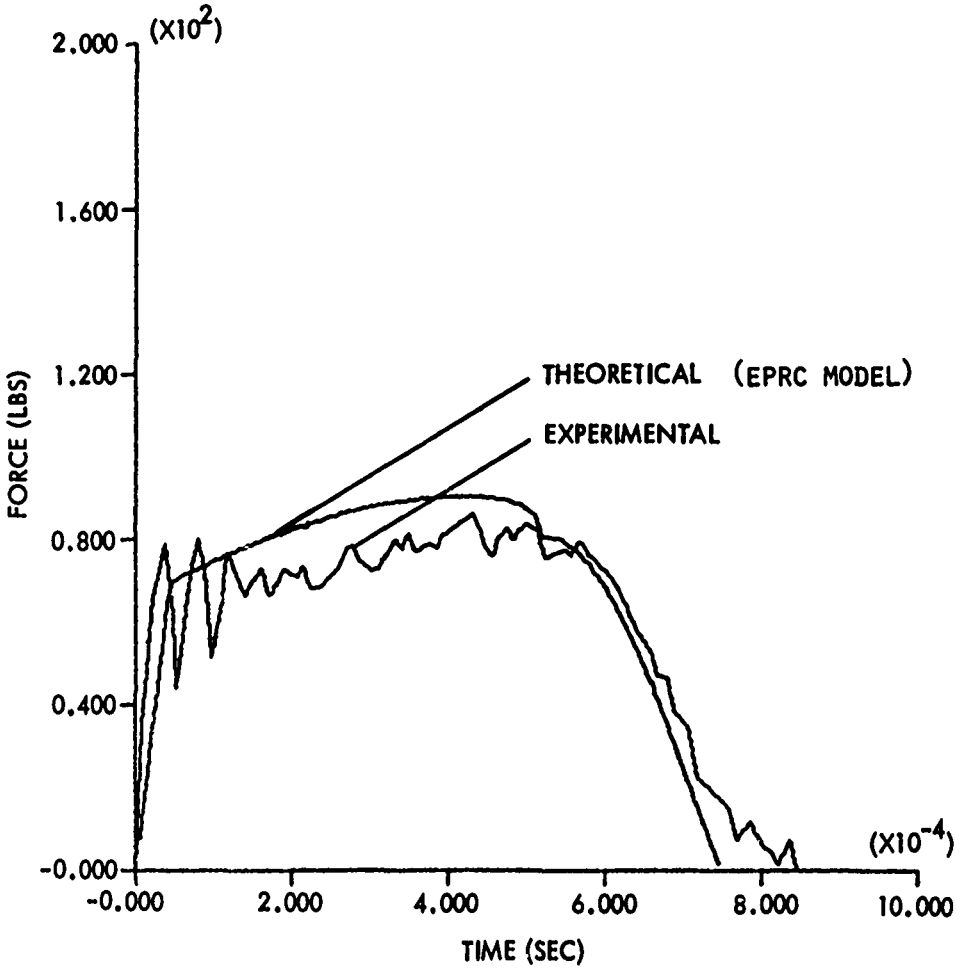

FIG. 28 TEST NO. 10

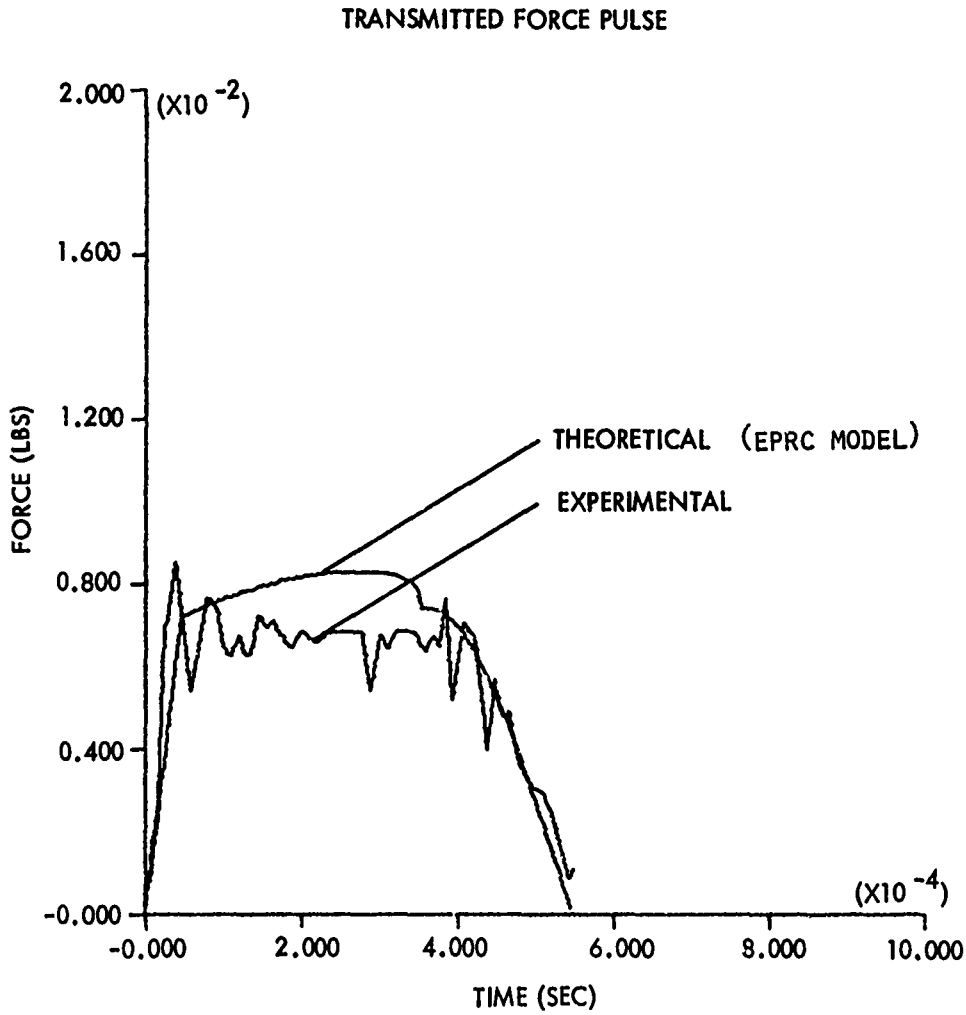

FIG. 29 - TEST NO. 11

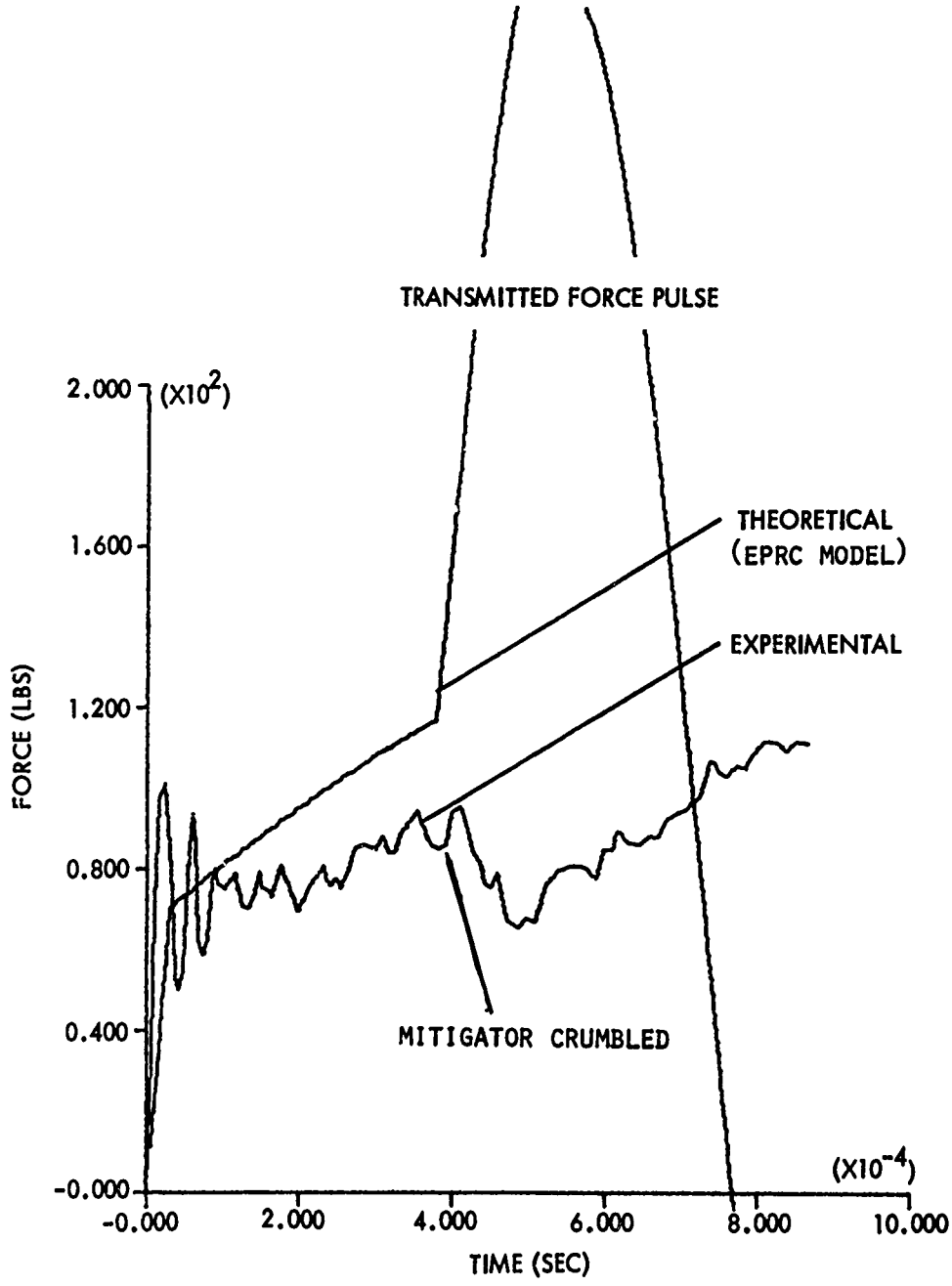

FIG. 30 TEST NO. 12

APPENDIX A

NUMERICAL INTEGRATION

Equations (A-1) and (A-2)

$$\varepsilon = \frac{1}{L}\left[U_o T - \int_o^T \int_o^t \frac{F}{M}\, dt dt - \int_o^T \frac{F}{(\rho g A)_{rod}}\, dt\right] \qquad \text{(A-1)}$$

$$\dot{\varepsilon} = \frac{1}{L}\left[U_o - \int_o^T \frac{F}{M}\, dt - \frac{F}{(\rho g A)_{rod}}\right] \qquad \text{(A-2)}$$

are numerically integrated using Equation (A-3)

$$F = F(\varepsilon, \dot{\varepsilon}, A) \qquad \text{(A-3)}$$

as a constraint. The integration is performed by applying a successive approximation method to a simple quadrature formula, the trapezoidal rule, Figure A-1. Equations A-1 and A-2 become

$$\varepsilon_n = \frac{1}{L}\left\{ U_o t_n - \frac{1}{2M} \sum_{i=1}^{n} \left[\sum_{i=1}^{n} (F_i + F_{i-1})\ (t_i - t_{i-1})\right] \right. \qquad \text{(A-4)}$$

$$\left. \left[t_i - t_{i-1}\right] - \frac{1}{2(\rho g A)_{rod}} \sum_{i=1}^{n} (F_i + F_{i-1})\ (t_i - t_{i-1}) \right\}$$

$$\dot{\varepsilon}_n = \frac{1}{L}\left\{U_o - \frac{1}{2M}\sum_{i=1}^{n}(F_i + F_{i-1})(t_i - t_{i-1}) - \frac{F_n}{(\rho g A)_{rod}}\right\} \quad \text{(A-5)}$$

for any time $0 \leq t_n \leq T$. At each new increment in time $t_n = t_{n-1} + \Delta t$, an estimate is made for the mitigator force F_n. Since the force is not changing very rapidly with time for much of the calculation, this assumed force is merely the F_n at the previous time t_{n-1}. The strain ε_n and strain-rate $\dot{\varepsilon}_n$ at time t_n are determined by evaluating Equations (A-4) and (A-5) using this F_n. A new force F_n is then calculated from Equation (A-3) using the new ε_n and $\dot{\varepsilon}_n$. The iteration is continued until the change in F_n becomes less than .1 percent of F_n. The results at time t_n are recorded, the time is advanced one time step and the entire procedure is repeated until F drops to zero.

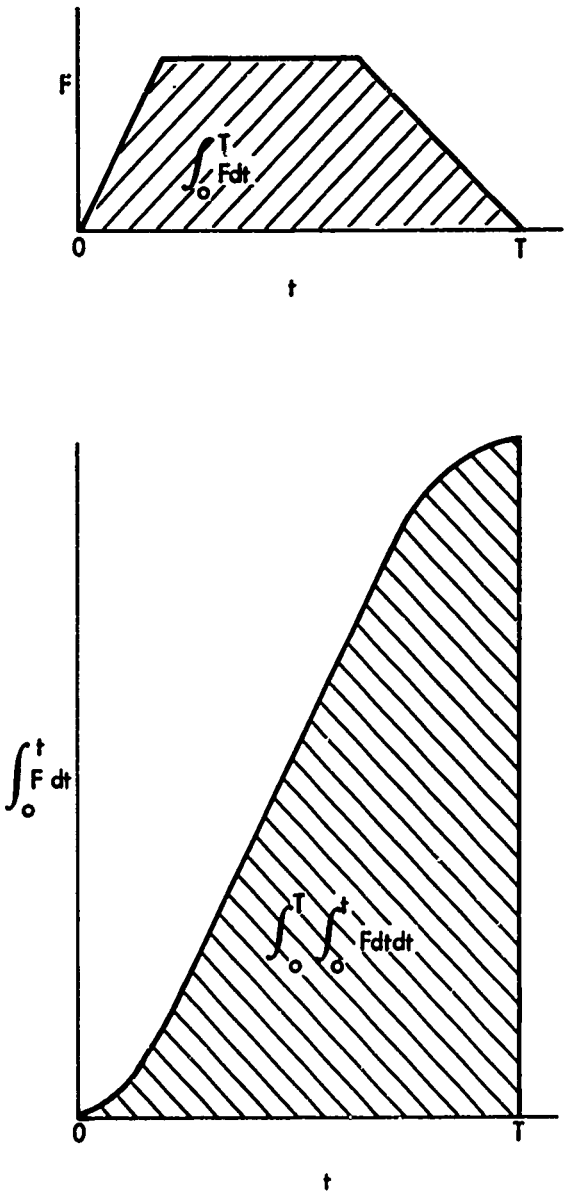

FIG. A-1 NUMERICAL INTEGRATION

APPENDIX B

COMPUTER PROGRAM LISTING

The computer program is written to handle the case of a rigid projectile impacting a semi-infinite elastic aluminum rod protected by a rigid polyurethane foam shock mitigator. It reduces the raw experimental data, calculates the equivalent theoretical results, and prints and plots the experimental and theoretical results.

```
      PROGRAM CBBOSCR(INPUT,OUTPUT,TAPE5=INPUT,TAPE6=OUTPUT,TAPE99)
    1 READ(5,2) NTEST,KOUT,NSPEC
    2 FORMAT(3I5)
C     NTEST = TEST IDENTIFICATION NUMBER
C     NTEST .LT. 0 -- STOPS RUN
C     KOUT = TYPE OF RUN
C     KOUT = 1 -- EXPERIMENTAL
C     KOUT = 2 -- THEORETICAL
C     KOUT = 3 -- EXPERIMENTAL AND THEORETICAL
C     NSPEC = SPECIMEN IDENTIFICATION NUMBER
      IF(NTEST.LT.0) GO TO 9999
      READ(5,22) SPECL,SPECD1,SPECD2,SPECRO,PROJWT,VELIMP,VELRB
   22 FORMAT(7F10.5)
C     SPECL = SPECIMEN LENGTH (IN)
C     SPECD1 = SPECIMEN DIAMETER (IMPACT FACE) (IN)
C     SPECD2 = SPECIMEN DIAMETER (REAR FACE) (IN)
C     SPECRO = SPECIMEN DENSITY (LBS/FT3)
C     PROJWT = PROJECTILE WEIGHT (LBS)
C     VELIMP = IMPACT VELOCITY (IN/SEC)
C     VELRB = REBOUND VELOCITY (IN/SEC)
      PROJEO = .5*PROJWT*VELIMP**2/386.
      PROJEF = .5*PROJWT*VELRB**2/386.
      CALL CALCM1(1,0.,0.,0,0.,0.001,0.,200.,5.,5.,
     123HTRANSMITTED FORCE PULSE,-23,
     210HTIME (SEC)      ,10,11HFORCE (LBS),11,0.,18)
      WRITE(6,3) NTEST
    3 FORMAT(1H1,11HTEST NUMBER;I7)
      WRITE(6,4) NSPEC,SPECL,SPECRO
    4 FORMAT(1H0,11HSPECIMEN NO,I5/11HLENGTH (IN),F10.3/
     122HDENSITY (LBS/CUBIC FT),F10.1)
      WRITE(6,5) PROJWT,VELIMP,PROJEO,PROJEF
    5 FORMAT(1H0,10HPROJECTILE/12HWEIGHT (LBS),F10.6/24HIMPACT VELOCITY
     1(IN/SEC),F10.0/24HINCIDENT ENERGY (IN-LBS),E10.4/23HREBOUND ENERGY
     2 (IN-LBS),E10.4)
      PROJWT = PROJWT/386.
      GO TO (1000,2000,1000),KOUT
 1000 CALL EXPMT(PROJEO,PROJEF)
      IF(KOUT.EQ.1) GO TO 3000
 2000 CALL THEO(VELIMP,PROJWT,PROJEO,SPECL,SPECD1,SPECD2,SPECRO)
 3000 GO TO 1
 9999 CALL CALCM1(0,0.)
      STOP
      END
```

```
      SUBROUTINE EXPMT(PROJEO,PROJEF)
      DIMENSION TIMEM(200),FORCEM(200)
      READ(5,1) NPTS,CNVRT,CNVRF
    1 FORMAT(1I5,2F10.5)
C     NPTS = NUMBER OF EXPERIMENTAL POINTS
C     CNVRT = CONVERSION FACTOR FOR TIME (INPUT UNITS TO SECONDS)
C     CNVRF = CONVERSION FACTOR FOR FORCE (INPUT UNITS TO LBS)
      DO 100 I=1,NPTS,4
      READ(5,2) TIMEM(I),FORCEM(I),TIMEM(I+1),FORCEM(I+1),TIMEM(I+2),
     1FORCEM(I+2),TIMEM(I+3),FORCEM(I+3)
    2 FORMAT(12X,8F6.0)
  100 CONTINUE
C     TIMEM(I) = DATA
C     FORCEM(I) = DATA
      FINT = 0.
      DO 200 I=1,NPTS
      TIMEM(I) = CNVRT*TIMEM(I)
      FORCEM(I) = CNVRF*FORCEM(I)
      IF (I.EQ.1) GO TO 200
      FINT = FINT+(FORCEM(I)**2+FORCEM(I-1)**2)*(TIMEM(I)-TIMEM(I-1))/2.
  200 CONTINUE
      ENGYTR = .102*FINT
      ENGYAB = PROJEO-PROJEF-ENGYTR
      CALL CALCM1(-NPTS,TIMEM,FORCEM,0)
      WRITE(6,3)
    3 FORMAT(1H-,20HEXPERIMENTAL RESULTS)
      WRITE(6,4)
    4 FORMAT(1H ,10HTIME (SEC)    ,10X,11HFORCE (LBS))
      DO 300 I=1,NPTS
      WRITE(6,5) TIMEM(I),FORCEM(I)
    5 FORMAT(1H ,2(1PE13.3))
  300 CONTINUE
      WRITE(6,6) ENGYAB,ENGYTR
    6 FORMAT(1H0,24HENERGY ABSORBED (IN-LBS),E10.4/
     127HENERGY TRANSMITTED (IN-LBS),E10.4)
      RETURN
      END
```

```
      SUBROUTINE THEO(U0,M1,PROJEO,L,D1,D2,RO)
      DIMENSION TIMEC(200),FORCEC(200),STRANC(200),RATEC(200)
     2,VPROJ(200),VBAR(200),ENGYAB(200),ENGYTR(200)
      REAL I,I0,I1,I2,M1,L
      READ(5,1) NCASE,STPSIZ
    1 FORMAT(I5,E15.5)
C     NCASE = TYPE OF MATERIAL MODEL
C     NCASE = 1 -- RIGID, PERFECTLY PLASTIC
C     NCASE = 2 -- RIGID, PERFECTLY PLASTIC, STRAIN RATE DEPENDENT
C     NCASE = 3 -- ELASTIC, PERFECTLY PLASTIC
C     NCASE = 4 -- ELASTIC, PERFECTLY PLASTIC, STRAIN RATE DEPENDENT
C     STPSIZ = TIME STEP (SECONDS)
      J = 0
      NPTSC = 0
      Z = 10.2
      D = STPSIZ
      T = D
      F = 0.
      F1 = 0.
      F5 = 0.
      F9 = 0.
      E9 = 0.
      I = 0.
      I0 = 0.
  110 DO 160 N=1,200
      I1 = I+(F+F1)*D/2.
      I2 = I0+(I+I1)*D/2.
      R1 = (U0-F1/Z)/L-I1/(L*M1)
      E1 = U0*T/L-I1/(L*Z)-I2/(L*M1)
      IF(NCASE.GT.2) GO TO 153
      CALL RIGID(NCASE,U0,L,D1,D2,RO,E1,R1,F1)
      IF(R1.LT.0.) GO TO 5000
      GO TO 155
  153 CALL ELASTC(NCASE,J,U0,L,D1,D2,RO,E1,E9,R1,S,F1,F9)
      IF(F1.LT.0.) GO TO 5000
  155 IF(ABS(1-F5/F1).LT..001) GO TO 170
      F5 = F1
  160 CONTINUE
  170 NPTSC = NPTSC+1
      TIMEC(NPTSC) = T
      FORCEC(NPTSC) = F1
      STRANC(NPTSC) = E1
      RATEC(NPTSC) = R1
      VPROJ(NPTSC) = U0-I1/M1
      VBAR(NPTSC) = F1/Z
      IF (NPTSC.NE.1) GO TO 175
      ENGYTR(1) = .102*FORCEC(1)**2*D/2.
      GO TO 176
  175 ENGYTR(NPTSC) = ENGYTR(NPTSC-1)+.102*(FORCEC(NPTSC)**2
     1+FORCEC(NPTSC-1)**2)*D/2.
  176 ENGYAB(NPTSC) = PROJEO-.5*M1*VPROJ(NPTSC)**2/386.-ENGYTR(NPTSC)
      IF (NPTSC.EQ.200) GO TO 5000
```

```
180 T = T+D
    F = F1
    I = I1
    I0 = I2
    IF(E1.LE.E9) GO TO 240
    E9 = E1
    F9 = F1
240 GO TO 110

5000 CALL CALCM1(-NPTSC,TIMEC,FORCEC,0)
     WRITE (6,2) NCASE,S
   2 FORMAT (1H-,19HTHEORETICAL RESULTS,10X,4HCASE,I5,10X,3HE =,F10.0)
     WRITE (6,3)
   3 FORMAT (1H ,10HTIME (SEC)     ,10X,11HFORCE (LBS),3X,
    214HSTRAIN (IN/IN),3X,12HRATE (1/SEC),3X,14HVPROJ (IN/SEC),3X,
    313HVBAR (IN/SEC),3X,11HEA (IN-LBS),3X,11HET (IN-LBS))
     DO 100 K=1,NPTSC
     WRITE (6,4) TIMEC(K),FORCEC(K),STRANC(K),RATEC(K),VPROJ(K),
    2VBAR(K),ENGYAB(K),ENGYTR(K)
   4 FORMAT (1H ,8(1PE15.3))
 100 CONTINUE
     RETURN
     END
```

```
      SUBROUTINE RIGID (NCASE,U0,L,D1,D2,R0,E1,R1,F1)
C     RIGID, PERFECTLY PLASTIC MATERIAL MODEL
      REAL L
      CALL AREA (A,D1,D2,E1)
      IF (NCASE.EQ.2) GO TO 550
      R5=U0/L
      GO TO 560
  550 R5=R1
  560 CALL STRATE(R0,R5,STRESS)
      F1 = A*STRESS
      RETURN
      END
```

```
      SUBROUTINE ELASTC(NCASE,J,U0,L,D1,D2,R0,E1,E9,R1,S,F1,F9)
C     ELASTIC, PERFECTLY PLASTIC MATERIAL MODEL
      REAL L
      CALL AREA (A,D1,D2,E1)
      CALL MOD(R0,S)
      IF (NCASE.EQ.4) GO TO 625
      R5=U0/L
      GO TO 630
  625 R5=R1
  630 IF (J.GT.0) GO TO 650
      CALL STRATE(R0,R5,STRESS)
      EYIELD = STRESS/S
      IF (E1.GT.EYIELD) GO TO 650
      F1 = S*E1*A
      GO TO 685
  650 IF (E1.LT.E9) GO TO 675
      IF (E1.GT..5) GO TO 675
      J = J+1
      IF (R1.LT.0.) GO TO 675
      CALL STRATE(R0,R5,STRESS)
      F1 = A*STRESS
      GO TO 685
  675 F1 = F9-S*(E9-E1)*A
  685 RETURN
      END
```

```
      SUBROUTINE MOD(RO,S)
C     DENSITY DEPENDENCE OF MODULUS
      S = 230.*RO**1.7
      RETURN
      END
```

```
      SUBROUTINE STRATE(RO,R5,STRESS)
C     STRAIN RATE AND DENSITY DEPENDENCE OF STRESS
      STRESS = (8.69+.306*ALOG(R5))*RO**1.69
      RETURN
      END
```

```
      SUBROUTINE AREA (A,D1,D2,E1)
C     STRESS AREA
      A=.7854*(D1+(D2-D1)*E1/.5)**2.
      RETURN
      END
```